Khoder *et al. Gut Pathogens* (2026) 18:27
https://doi.org/10.1186/s13099-026-00814-8

Gut Pathogens

RESEARCH Open Access

# Novel indole-based sulfonate and sulfamate derivatives as potent and selective urease inhibitors targeting *Helicobacter pylori*: a promising therapeutic strategy

Ghalia Khoder[1,2*†], Esra M. Mustafa[1†], Sumera Zaib[3*], Anil Ravi[1], Afnan I. Shahin[1], Seyed-Omar Zaraei[1], Nehal Rana[3], Hanan S. Anbar[4], Hafiz Saqib Ali[5], Shamsul Qumar[1], Merylin Sebastian[1], Ragheb Alsheikh Zein[1] and Mohammed I. El-Gamal[6,7*]

## Abstract

*Helicobacter pylori* (*H. pylori*) infection is strongly associated with peptic ulcer and gastric cancer, compounded by the growing prevalence of antibiotic resistance. Current antibiotic eradication therapies often lead to gut dysbiosis and treatment failure, highlighting the urgent need for targeted, alternative therapies. In this study, a novel series of indole-based heterocycles bearing sulfonate or sulfamate functionalities was designed, synthesized, and evaluated as potential urease inhibitors. Several derivatives exhibited potent urease inhibition using a cell-free urease assay, with compound 1n emerging as the most active inhibitor ($IC_{50}$ = 0.23 ± 0.33 µM), approximately 100-fold more potent than thiourea ($IC_{50}$ = 23.2 ± 11.0 µM). Antibacterial screening confirmed significant activity against *H. pylori*, particularly for compounds 1k (MIC < 1.5 µM) and 1 h (MIC = 2.31 ± 1.15 µM), both of which also demonstrated direct and significant inhibition of *H. pylori* urease in vitro. These compounds displayed remarkable selectivity, showing no inhibitory effect on *E. coli* and six *Lactobacillus* strains, suggesting a beneficial role in maintaining gut microflora unlike conventional antibiotic therapy. Furthermore, cytotoxicity assays on human gastric epithelial (AGS) and dermal fibroblast (F180) cells confirmed minimal toxicity, while Caco-2 permeability studies indicated low systemic absorption, suggesting localized gastrointestinal activity. Molecular docking revealed strong interactions of 1 h and 1k within the *H. pylori* urease active site. In silico ADMET analysis predicted low CNS toxicity, moderate CYP450 inhibition, and absence of PAINS alerts. Overall, these findings identify promising lead molecules for the development of potent, selective, and safer urease inhibitors against *H. pylori*.

†Ghalia Khoder and Esra M. Mustafa contributed equally to this work and Co-first authors.

*Correspondence:
Ghalia Khoder
gkhoder@sharjah.ac.ae
Sumera Zaib
sumera.zaib@ucp.edu.pk
Mohammed I. El-Gamal
drmelgamal2002@gmail.com

Full list of author information is available at the end of the article

**Keywords** Helicobacter pylori, Indole-Based Sulfonate and Sulfamate Derivatives, Urease Inhibitors, Antibiotic resistance

**Graphical abstract**

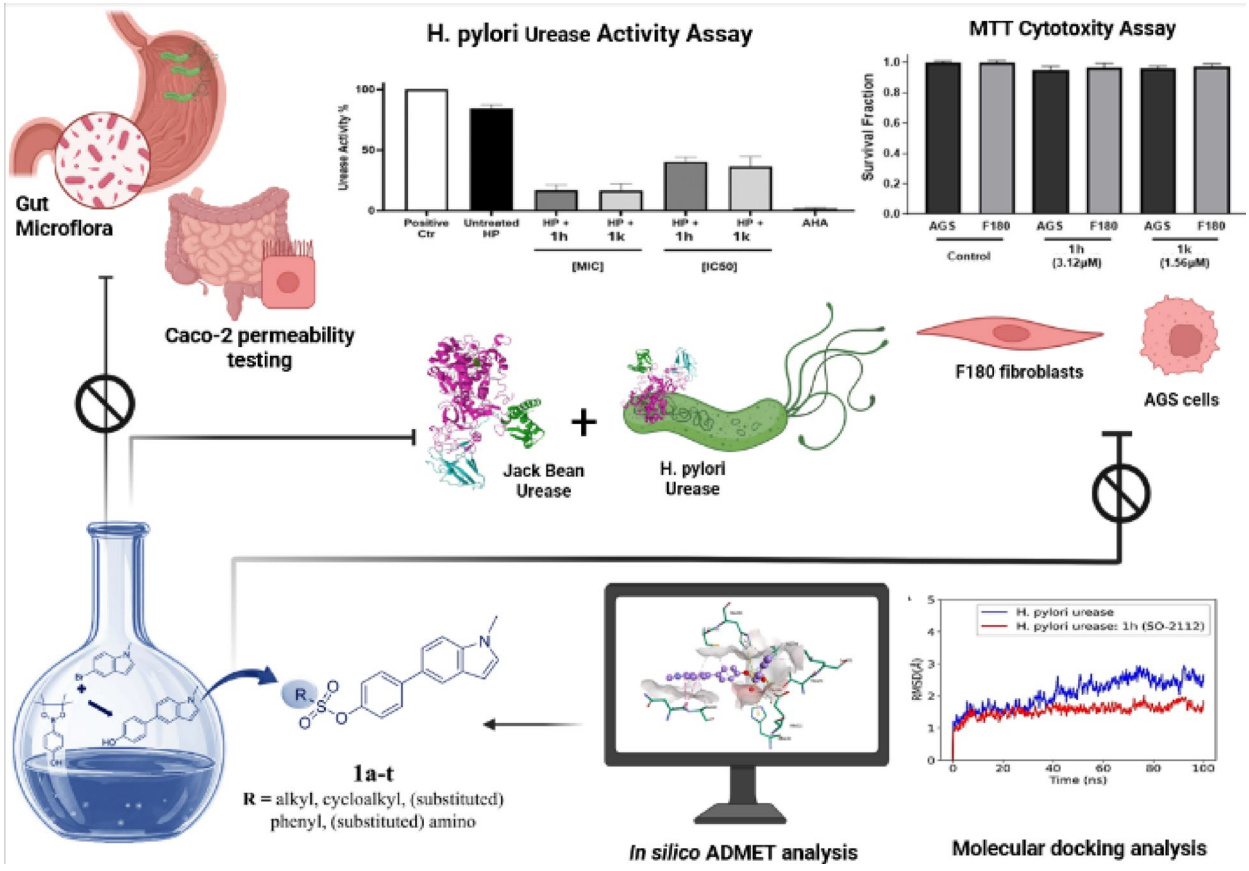


## Introduction

Urease is a nickel-dependent metalloenzyme that catalyzes the hydrolysis of urea into ammonia and carbamate [Fig. 1], thereby providing a critical nitrogen source for various bacterial species [1–4]. Notably, urease was the first enzyme shown to require nickel ions as an essential catalytic cofactor [5]. Since its discovery, extensive research has elucidated urease's pivotal role in the biogeochemical nitrogen cycle. Moreover, urease has been recognized as a key virulence factor in several pathogenic bacteria, including *Proteus mirabilis*, *Klebsiella pneumoniae*, and *Helicobacter pylori*. In the urinary tract, urease activity elevates local pH through ammonia production, promoting the formation of struvite stones. These stones can obstruct the urinary tract, impair antibiotic efficacy, and facilitate persistent bacterial colonization [1, 5, 6]. This pathogenic process is regulated by pH and depends on a proton-gated urea channel that promotes urea uptake under acidic conditions, thereby enabling urease activity at pH values as low as 2.5 [7]. In *H. pylori*, urease plays a central role in gastric mucosal colonization, contributing to the development of gastrointestinal pathologies such as peptic ulcers and potentially gastric cancer [8]. The ammonia generated by urease exerts cytotoxic effects through direct epithelial damage and by promoting neutrophil-mediated cellular injury [1, 5]. Given urease's critical involvement in microbial survival and pathogenesis, particularly in hostile acidic or urea-rich environments, its inhibition represents a promising therapeutic strategy. Targeting urease could disrupt bacterial colonization, prevent disease progression, and enhance the efficacy of conventional antimicrobial treatments [9].

Urease-catalyzed hydrolysis of urea to ammonia and carbamate (carbamic acid); the carbamate then hydrolyzes non-enzymatically to carbonic acid, releasing a second equivalent of $NH_3$ [9]. As shown in Fig. 2, urease exhibits a trimeric quaternary structure composed of three $[(\alpha\beta\gamma)_3]_4$ units, each harbouring three active sites located within the α subunits. Each active site contains a dinuclear nickel center, with two closely spaced Ni atoms [Ni(1) and Ni(2)] separated by approximately 3.5 Å [10].

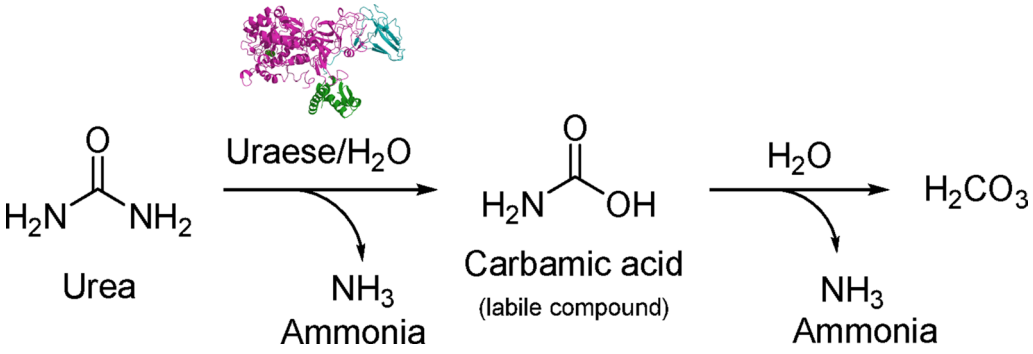


**Fig. 1** Mechanism of urease-mediated urea hydrolysis

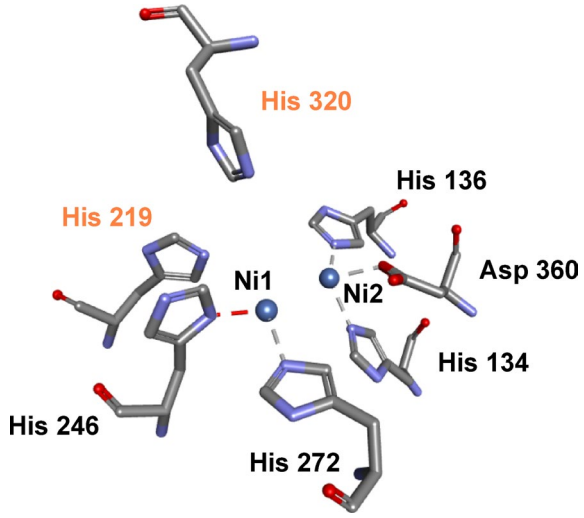


**Fig. 2** Structure of the urease active site

A carbamylated lysine residue (αLys217*) bridges the two nickel ions through its Oθ1 and Oθ2 atoms, consistent with the requirement for carbon dioxide in vitro to facilitate lysine carbamylation and urease activation [11]. The catalytic activity of urease is intricately regulated through metal ion coordination and protein-protein interactions. The insertion of nickel ions into the active site is not spontaneous but is orchestrated by a dedicated set of accessory proteins and chaperones, ensuring precise metallocenter assembly and enzymatic activation [12]. Additionally, in *H. pylori*, the *ure* gene cluster typically consists of seven genes. *ureA* and *ureB* encode the structural subunits of the enzyme, while *ureE*, *ureF*, *ureG*, and *ureD* function as accessory genes involved in inserting nickel ions into the active site, which is important for catalytic activity [2, 13]. The holoenzyme is composed of six copies of each subunit, with two nickel ions required per active site, which are located within the *ureB* subunit [14]. Catalytic activity relies on the proper coordination of these nickel ions within the protein structure. Although the enzyme can assemble without nickel ions or accessory proteins, it remains inactive [2, 15].

The urease active site comprises two nickel ions (blue spheres) bridged by carboxylated lysine and a hydroxide ion. Ni1 is ligated by His219, His246, and His272, whereas Ni2 is ligated by His134, His136, and Asp360; His320 is positioned nearby above the dinickel center. Oxygen atoms are colored red, nitrogen blue, and carbon gray; coordinating side chains are shown with gray carbons, with selected histidines highlighted in orange [12].

Recently, increasing attention has been directed toward the development of urease inhibitors, particularly in response to the growing issue of antibiotic resistance in *H. pylori*. To address this challenge, a wide range of heterocyclic and non-heterocyclic compounds have been synthesized with the aim of counteracting the pathogenic effects of urease-producing bacteria [Fig. 3]. Hydroxamic acids, such as acetohydroxamic acid (AHA, I), are classical inhibitors that chelate the active-site nickel and significantly reduce enzyme activity, though clinical use is limited by toxicity [16]. Phosphoramidates and phosphonic acids (II) act as transition state analogues and show strong nickel-binding properties [17]. Thioureas and isothioureas (III) mimic the urea substrate and have shown moderate but specific urease inhibition III [18]. Schiff bases, particularly those containing thiazole and hydrazone motifs IV, have gained attention for their favorable urease inhibition profiles, likely due to their ability to coordinate metal centers in the enzyme [19]. Natural products, especially flavonoids and polyphenols like quercetin (V) and baicalin, exhibit significant inhibitory effects, often through hydrogen bonding and π-interactions within the urease active site [20, 21]. In addition, sulfonates and sulfamates analogues have shown significant promise for urease inhibition. For instance, sulfonates and sulfamates bearing imidazo[2,1-*b*]thiazole scaffold (VI) that exhibit a potent inhibitory activity of urease enzyme have demonstrated remarkable inhibitory effects [22]. Similarly, sulfonate and sulfamate derivatives bearing benzofuran (VII) or benzothiophene (VIII) scaffolds exhibited potent urease inhibition [23]. Moreover, Indole-3-carbaldehyde oximes (IX) evaluated as urease inhibitors against *H. pylori* [24]. Recent

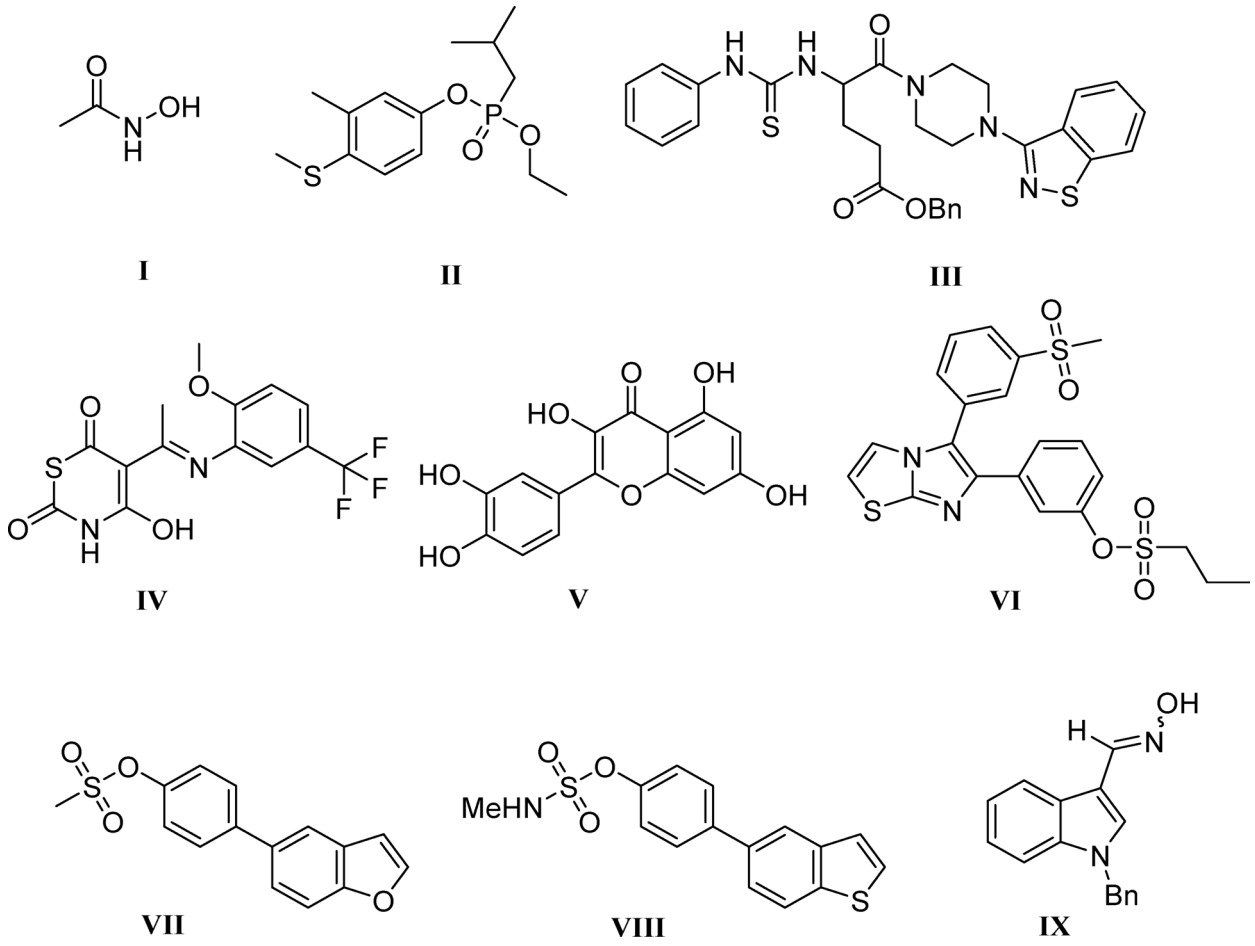


**Fig. 3** Structures of urease inhibitors in literature [16–24]

advances in computational techniques, including molecular docking and molecular dynamics simulations, have further enhanced the understanding of urease–ligand interactions and facilitated the optimization of inhibitor design [25]. Collectively, these diverse chemotypes provide a valuable foundation for the continued development of novel urease inhibitors with therapeutic potential in the treatment of *H. pylori* infections.

Sulfonates and sulfamates are well-established as biocompatible medicinal groups that have gained significant prominence within pharmaceutical compound libraries. Their incorporation into bioactive structures has been thoroughly explored, particularly for the therapeutic inhibition of these key metalloenzymes [22, 23, 26, 27]. These enzymes play essential roles in numerous physiological and pathological pathways, making them attractive targets in drug discovery. Our previously published work demonstrated that benzo[*b*]furan and benzo[*b*] thiophene scaffolds functionalized with sulfonate and sulfamate moieties exhibit potent urease inhibitory activity [23, 26, 28]. Building upon these findings, the present work reports the rational design and development of novel sulfonate and sulfamate analogues targeting urease. Our research specifically focused on the synthesis and comprehensive biological evaluation of indole-based sulfonate and sulfamate derivatives. The biological potential of the synthesized compounds was systematically investigated using a multifaceted analytical strategy, incorporating enzymatic inhibition assays, antibacterial activity profiling, structure-activity relationship (SAR) analysis, and molecular modelling studies [29–32]. Through these approaches, our aim is to identify promising lead compounds with significant potential for therapeutic applications in urease-targeted antimicrobial strategies.

## Materials and methods

### General

Starting materials 5-bromo-1-methyl-1*H*-indole (2), 4-(4,4,5,5-tetramethyl-1,3,2-dioxaborolan-2-yl) phenol (3), various sulfonyl and sulfamoyl chlorides were sourced from Sigma-Aldrich (Schnelldorf, Germany) and BLD Pharma (Beijing, China). The chemical transformations were conducted in oven-dried glassware

under nitrogen. Distillation was performed on all solvents prior to their employment in purification and isolation processes involving column chromatography (200–400 mesh). Reaction progress was monitored using TLC (thin-layer chromatography) on 0.25 mm silica gel plates (E. Merck, 60 F 254) and visualized the results with iodine and a UV lamp. $^{1}$H and $^{13}$ C NMR spectra were acquired using a Bruker 500 MHz spectrometer. Chemical shifts are expressed in ppm, with spin multiplicities and coupling constants (in Hz) specified for their corresponding peaks. HRMS analysis was performed on a BRUKER TIMS TOF high resolution mass spectrometer and finally, melting points were measured using Stuart SMP50 (Staffordshire, UK) digital instrument.

The urease inhibition assay was conducted using a jack bean urease kit, with thiourea, urea, $K_2HPO_4$, LiCl, and EDTA purchased from Sigma-Aldrich. *H. pylori* ATCC 43,504 (DSM 21031) was acquired from the German Collection of Microorganisms and Cell Cultures (DSMZ), Braunschweig, Germany. Bacterial and cell culture media-including Brucella agar, RPMI, fetal bovine serum (FBS), horse serum, and acetohydroxamic acid (AHA; CAS No. 546-88-3) were purchased from Sigma- Aldrich (USA). For the microaerophilic cultivation of *H. pylori*, a CampyGen 2.5 L gas-generating pack (Oxoid, Thermo Scientific, UK) and an anaerobic jar (bioMérieux, France) were used. Bacterial suspension densities were standardized employing the DensiCHEK PLUS (bioMérieux, France), and optical density (OD) was measured at 570–600 nm using a Synergy H1 microplate reader (BioTek, USA). The half-maximal inhibitory concentration ($IC_{50}$) was calculated using GraphPad Prism version 8.0.2 (GraphPad Inc., La Jolla, CA, USA). Minimum inhibitory concentrations (MICs) were determined by the agar dilution method, in accordance with Clinical and Laboratory Standards Institute (CLSI M07, 2019) guidelines.

### Experimental procedure for the synthesis of target compounds (1a-t)

The synthetic method, experimental conditions, and characterization details align with our earlier study [23].

#### *Experimental procedure for the synthesis of intermediate N-methylindole compound (4)*

To a stirred solution of 5-bromo-1-methyl-1H-indole (**2**) (400 mg, 1.9 mmol, 1.0 eq.), (4,4,5,5-tetramethyl-1,3,2-dioxaborolan-2-yl)phenol (**3**) (502 mg, 2.28 mmol, 1.2 eq.) in 1,4-dioxane (12 mL) and $H_2O$ (6 mL) added $K_2CO_3$ (1.05 g, 7.62 mmol, 4 eq.) and purged the reaction system with $N_2$. After 5 min, $PdCl_2$(dppf) (111 mg, 0.15 mmol, 0.08 eq.) was added and the reaction mixture was stirred under MW at 120 °C. After 2 h, the reaction mixture was diluted with the reaction mixture was diluted with EtOAc (30 mL) and $H_2O$ (10 mL) and then organic layer was separated and subjected to sequential washes with $H_2O$ (30 mL) and followed by sat. aq. NaCl solution (20 mL). Subsequently, the organic phase was dried over anhydrous $Na_2SO_4$, filtered, and concentrated under reduced pressure. Purification was performed using normal phase column chromatography with mobile phase ethyl acetate: hexane 12:88 *v/v*; Yield: 64%; $^{1}$H NMR (500 MHz, Acetone-$d_6$) δ 8.31 (s, 1H), 7.73 (d, $J$ = 0.6 Hz, 1H), 7.49 (d, $J$ = 8.4 Hz, 2 H), 7.41–7.30 (m, 2 H), 7.21 (d, $J$ = 3.1 Hz, 1H), 6.90 (d, $J$ = 8.4 Hz, 2 H), 6.45 (d, $J$ = 3.1 Hz, 1H), 3.84 (s, 3 H); $^{13}$C NMR (126 MHz, Acetone-$d_6$) δ 157.1, 137.0, 134.9, 133.3, 130.5, 130.2, 128.9, 121.4, 119.0, 116.4, 116.3, 110.4, 101.7, 32.9, ESI-MS m/z: [M + H] $^{+}$ 223.94.

#### *General experimental procedure for the synthesis of indole sulfonate compounds (1a-o)*

To a stirred solution of compound **4** (40 mg, 0.18 mmol, 1.0 eq.) and TEA (0.25 mL, 10.0 eq.) in DCM (2 mL) added dropwise addition of appropriate sulfonyl chloride (0.9 mmol, 5 eq.) in DCM (1 mL) at 0 °C under a nitrogen atmosphere over 10 min and stirred at rt. Ater 12 h, the reaction was quenched using Sat. aq. $NaHCO_3$ solution and separated the DCM layer and subjected to sequential washes with $H_2O$ (5 mL) and followed by sat. aq. NaCl solution (5 mL). Subsequently, the organic phase was dried over anhydrous $Na_2SO_4$, filtered, and concentrated under reduced pressure. Further purification was carried out by trituration method using diethyl ether and *n*-pentane to afford the compounds **1a-f** in good yields (47–91%).

**4-(1-Methyl-1 H-indol-5-yl) phenyl ethane sulfonate (1a)** Trituration was performed using diethyl ether and *n*-pentane (1:5) *v/v*; Yield: 80%; Pale green color solid; mp:143–145 °C; $^{1}$H NMR (500 MHz, $CDCl_3$) δ 7.80 (d, $J$ = 1.1 Hz, 1H), 7.68–7.64 (m, 2 H), 7.43 (dd, $J$ = 8.5, 1.7 Hz, 1H), 7.39 (d, $J$ = 8.5 Hz, 1H), 7.35–7.31 (m, 2 H), 7.10 (d, $J$ = 3.1 Hz, 1H), 6.54 (dd, $J$ = 3.1, 0.6 Hz, 1H), 3.83 (s, 3 H), 3.32 (q, $J$ = 7.4 Hz, 2 H), 1.57 (t, $J$ = 7.5 Hz, 3 H); $^{13}$C NMR (126 MHz, $CDCl_3$) δ 148.0, 142.0, 136.5, 131.5, 129.9, 129.1, 128.9, 122.2, 121.4, 119.6, 109.7, 101.5, 45.0, 33.1, 8.4; HRMS (ESI-TOF): m/z [M + H]$^{+}$ calcd for $C_{17}H_{17}NO_3S$, 316.1002 found 316.1003.

**4-(1-Methyl-1 H-indol-5-yl) phenyl propane-1-sulfonate (1b)** Trituration was performed using diethyl ether and *n*-pentane(1:6) *v/v*; Yield: 68%; brown color solid; mp: 76–78 °C; $^{1}$H NMR (500 MHz, $CDCl_3$) δ 7.80 (d, $J$ = 1.2 Hz, 1H), 7.68–7.64 (m, 2 H), 7.43 (dd, $J$ = 8.5, 1.7 Hz, 1H), 7.39 (d, $J$ = 8.5 Hz, 1H), 7.35–7.30 (m, 2 H), 7.10 (d, $J$ = 3.1 Hz, 1H), 6.54 (dd, $J$ = 3.1, 0.6 Hz, 1H), 3.83 (s, 3 H), 3.28–3.24 (m, 2 H), 2.10–2.01 (m, 2 H), 1.14 (t, $J$ = 7.5 Hz, 3 H); $^{13}$C NMR (126 MHz, $CDCl_3$) δ 148.0, 142.0, 136.5, 131.6,

129.9, 129.1, 128.9, 122.3, 121.4, 119.6, 109.7, 101.5, 52.1, 33.1, 17.5, 13.1; HRMS (ESI-TOF): m/z $[M+H]^+$ calcd for $C_{18}H_{19}NO_3S$, 330.1159 found 330.1159.

**4-(1-Methyl-1 H-indol-5-yl) phenyl propane-2-sulfonate (1c)** Trituration was performed using diethyl ether and *n*-pentane(1:6) *v/v*; Yield: 91%; Pale brown color solid; mp: 155–157 °C; $^1$H NMR (500 MHz, $CDCl_3$) δ 7.80 (d, *J* = 1.1 Hz, 1H), 7.68–7.63 (m, 2 H), 7.45–7.41 (m, 1H), 7.39 (d, *J* = 8.5 Hz, 1H), 7.35–7.31 (m, 2 H), 7.10 (d, *J* = 3.1 Hz, 1H), 6.54 (dd, *J* = 3.1, 0.6 Hz, 1H), 3.83 (s, 3 H), 3.56–3.46 (m, 1H), 1.58 (d, *J* = 6.9 Hz, 6 H); $^{13}$C NMR (126 MHz, $CDCl_3$) δ 147.9, 141.8, 136.5, 131.6, 129.8, 129.1, 128.8, 122.2, 121.4, 119.6, 109.7, 101.5, 52.5, 33.1, 16.9; HRMS (ESI-TOF): m/z $[M+H]^+$ calcd for $C_{18}H_{19}NO_3S$, 330.1159 found 330.1160.

**4-(1-Methyl-1 H-indol-5-yl) phenyl butane-1-sulfonate (1d)** Trituration was performed using diethyl ether and *n*-pentane(1:5) *v/v*; Yield: 77%; Pale brown color solid; mp: 157–159 °C; $^1$H NMR (500 MHz, $CDCl_3$) δ 7.80 (d, *J* = 1.2 Hz, 1H), 7.68–7.63 (m, 2 H), 7.43 (dd, *J* = 8.5, 1.7 Hz, 1H), 7.39 (d, *J* = 8.5 Hz, 1H), 7.35–7.31 (m, 2 H), 7.10 (d, *J* = 3.1 Hz, 1H), 6.54 (dd, *J* = 3.0, 0.4 Hz, 1H), 3.83 (s, 3 H), 3.33–3.24 (m, 2 H), 2.05–1.94 (m, 2 H), 1.59–1.49 (m, 2 H), 1.00 (t, *J* = 7.4 Hz, 3 H); $^{13}$C NMR (126 MHz, $CDCl_3$) δ 148.0, 142.0, 136.5, 131.6, 129.9, 129.1, 128.8, 122.3, 121.4, 119.6, 109.7, 101.5, 50.2, 33.1, 25.6, 21.6, 13.7; HRMS (ESI-TOF): m/z $[M+H]^+$ calcd for $C_{19}H_{21}NO_3S$, 344.1315 found 344.1315.

**4-(1-Methyl-1 H-indol-5-yl)phenyl cyclopropane sulfonate (1e)** Trituration was performed using diethyl ether and *n*-pentane(1:5) *v/v*; Yield: 58%; Pale green color solid; mp: 126–128 °C; $^1$H NMR (500 MHz, $CDCl_3$) δ 7.81 (d, *J* = 1.2 Hz, 1H), 7.68–7.63 (m, 2 H), 7.43 (dd, *J* = 7.1, 3.5 Hz, 1H), 7.41–7.34 (m, 3 H), 7.10 (d, *J* = 3.1 Hz, 1H), 6.54 (d, *J* = 2.6 Hz, 1H), 3.83 (s, 3 H), 2.66–2.60 (m, 1H), 1.35–1.29 (m, 2 H), 1.17–1.10 (m, 2 H); $^{13}$C NMR (126 MHz, $CDCl_3$) δ 148.5, 141.9, 136.5, 131.5, 129.9, 129.1, 128.7, 122.5, 121.3, 119.6, 109.7, 101.5, 33.1, 27.8, 6.4; HRMS (ESI-TOF): m/z $[M+H]^+$ calcd for $C_{18}H_{17}NO_3S$, 328.1002 found 328.1004.

**4-(1-Methyl-1 H-indol-5-yl) phenyl cyclohexyl sulfonate (1f)** Trituration was performed using diethyl ether and *n*-pentane (1:5) *v/v*; Yield: 47%; off white color solid; mp: 170–172 °C; $^1$H NMR (500 MHz, $CDCl_3$) δ 7.80 (d, *J* = 1.2 Hz, 1H), 7.67–7.63 (m, 2 H), 7.43 (dd, *J* = 8.5, 1.7 Hz, 1H), 7.38 (d, *J* = 8.5 Hz, 1H), 7.34–7.29 (m, 2 H), 7.10 (d, *J* = 3.1 Hz, 1H), 6.55–6.52 (m, 1H), 3.83 (s, 3 H), 3.30–3.20 (m, 1H), 2.43–2.33 (m, 2 H), 2.01–1.93 (m, 2 H), 1.82–1.70 (m, 3 H), 1.41–1.28 (m, 3 H); $^{13}$C NMR (126 MHz, $CDCl_3$) δ 147.9, 141.7, 136.5, 131.7, 129.8, 129.1, 128.8, 122.3, 121.4, 119.6, 109.7, 101.5, 60.5, 60.1, 33.1, 26.7, 25.2; HRMS (ESI-TOF): m/z $[M+H]^+$ calcd for $C_{21}H_{23}NO_3S$, 370.1472 found 370.1483.

**4-(1-Methyl-1 H-indol-5-yl)phenyl benzenesulfonate (1 g)** Trituration was performed using diethyl ether and *n*-pentane(1:5) *v/v*; Yield: 49%; off white color solid; mp: 112–114 °C; $^1$H NMR (500 MHz, $CDCl_3$) δ 7.90 – 7.87 (m, 2 H), 7.77–7.75 (m, 1H), 7.70–7.65 (m, 1H), 7.57–7.51 (m, 4 H), 7.39 (dd, *J* = 8.5, 1.7 Hz, 1H), 7.36 (d, *J* = 8.5 Hz, 1H), 7.09 (d, *J* = 3.1 Hz, 1H), 7.04–7.00 (m, 2 H), 6.53–6.51 (m, 1H), 3.82 (s, 3 H); $^{13}$C NMR (126 MHz, $CDCl_3$) δ 148.4, 141.9, 136.5, 135.7, 134.3, 131.5, 129.9, 129.3, 129.1, 128.7, 128.5, 122.6, 121.3, 119.6, 109.7, 101.5, 33.1; HRMS (ESI-TOF): m/z $[M+H]^+$ calcd for $C_{21}H_{17}NO_3S$, 364.1002 found 364.1001.

**4-(1-Methyl-1 H-indol-5-yl)phenyl 4-methylbenzenesulfonate (1 h)** Trituration was performed using diethyl ether and *n*-pentane(1:5) *v/v*; Yield: 59%; Pale pink color solid; mp: 146–148 °C; 1H NMR (500 MHz, $CDCl_3$) $^1$H NMR (500 MHz, $CDCl_3$) δ 7.77–7.73 (m, 3 H), 7.56–7.51 (m, 2 H), 7.40 (dd, *J* = 8.5, 1.7 Hz, 1H), 7.36 (d, *J* = 8.5 Hz, 1H), 7.32 (t, *J* = 6.0 Hz, 2 H), 7.09 (d, *J* = 3.1 Hz, 1H), 7.04–7.01 (m, 2 H), 6.52 (dd, *J* = 3.1, 0.6 Hz, 1H), 3.82 (s, 3 H), 2.46 (s, 3 H); $^{13}$C NMR (126 MHz, $CDCl_3$) δ 148.5, 145.4, 141.7, 136.5, 132.7, 131.5, 129.9, 129.8, 129.1, 128.8, 128.4, 122.6, 121.3, 119.6, 109.7, 101.5, 33.1, 21.9; HRMS (ESI-TOF): m/z $[M+H]^+$ calcd for $C_{22}H_{19}NO_3S$, 378.1159 found 378.1160.

**4-(1-Methyl-1 H-indol-5-yl)phenyl 4-(tert-butyl)benzenesulfonate (1i)** Trituration was performed using diethyl ether and *n*-pentane(1:5) *v/v*; Yield: 41%; white color solid; mp 123–125 °C; $^1$H NMR (500 MHz, $CDCl_3$) δ 7.82–7.78 (m, 2 H), 7.77 (dd, *J* = 1.6, 0.6 Hz, 1H), 7.56–7.52 (m, 4 H), 7.40 (dd, *J* = 8.5, 1.7 Hz, 1H), 7.36 (d, *J* = 8.5 Hz, 1H), 7.09 (d, *J* = 3.1 Hz, 1H), 7.07–7.03 (m, 2 H), 6.52 (dd, *J* = 3.1, 0.6 Hz, 1H), 3.82 (s, 3 H), 1.35 (s, 9 H); $^{13}$C NMR (126 MHz, $CDCl_3$) δ 148.4, 141.8, 139.6, 136.5, 135.5, 135.1, 131.5, 129.9, 129.1, 128.9, 128.5, 125.9, 122.6, 121.3, 119.6, 109.7, 101.5, 33.1, 29.8, 21.4; HRMS (ESI-TOF): m/z $[M+H]^+$ calcd for $C_{25}H_{25}NO_3S$, 420.1628 found 420.1626.

**4-(1-Methyl-1 H-indol-5-yl)phenyl 4-fluorobenzenesulfonate (1j)** Trituration was performed using diethyl ether and *n*-pentane(1:6) *v/v*; Yield: 40%; dark green color solid; mp: 123–125 °C; $^1$H NMR (500 MHz, $CDCl_3$) δ 7.92–7.87 (m, 2 H), 7.77 (dd, *J* = 1.6, 0.7 Hz, 1H), 7.57–7.53 (m, 2 H), 7.40 (dd, *J* = 8.5, 1.7 Hz, 1H), 7.37 (d, *J* = 8.5 Hz, 1H), 7.24–7.20 (m, 2 H), 7.09 (d, *J* = 3.1 Hz, 1H), 7.05–7.01 (m, 2 H), 6.52 (dd, *J* = 3.1, 0.6 Hz, 1H), 3.82 (s, 3 H); $^{13}$C NMR (126 MHz, $CDCl_3$) δ 167.2, 166.2 (d, J = 257.4 Hz), 165.1, 148.2, 142.0, 136.6, 131.7, 131.6 (d, J = 10.0 Hz),

131.6, 131.6, 131.4, 129.9, 129.1, 128.6, 122.5, 121.3, 119.6, 116.8, 116.7 (d, J = 22.8 Hz), 116.6, 109.7, 101.5, 77.4, 77.2, 76.9, 33.1; HRMS (ESI-TOF): m/z $[M+H]^+$ calcd for $C_{21}H_{16}FNO_3S$, 382.0908 found 382.0908.

**4-(1-Methyl-1 H-indol-5-yl phenyl 4-(trifluoromethyl) benzenesulfonate (1k)** Trituration was performed using diethyl ether and *n*-pentane (1:4) *v/v*; Yield: 48%; off white color solid; mp: 120–122 °C; $^1$H NMR (500 MHz, $CDCl_3$) δ 8.02 (d, *J* = 8.2 Hz, 2 H), 7.82 (d, *J* = 8.3 Hz, 2 H), 7.77 (d, *J* = 0.8 Hz, 1H), 7.59–7.55 (m, 2 H), 7.41–7.35 (m, 2 H), 7.09 (d, *J* = 3.1 Hz, 1H), 7.06–7.02 (m, 2 H), 6.52 (d, *J* = 3.0 Hz, 1H), 3.82 (s, 3 H); $^{13}$C NMR (126 MHz, $CDCl_3$) δ 148.1, 142.3, 139.3, 136.6,136.3, 135.9 (q, $J_{CF}$ = 33.3 Hz) 135.8, 135.5,131.2, 129.9, 129.3, 129.1, 128.7, 126.5 (d, $J_{CF}$ = 3.7 Hz), 126.4, 124.2, 123.2, (q, $J_{CF}$ = 260.2 Hz). 122.4, 121.2, 119.8,119.6, 109.8, 101.6, 33.1; HRMS (ESI-TOF): m/z $[M+H]^+$ calcd for $C_{22}H_{16}F_3NO_3S$, 432.0876 found 432.0879.

#### *4-(1-Methyl-1 H-indol-5-yl)phenyl 3-methylbenzenesulfonate (1 L)*

Purification was performed using normal column chromatography at 10% Ethyl acetate and Hexane; Yield: 70%; off white color solid; mp: 102–104 °C; $^1$H NMR (500 MHz, $CDCl_3$) δ 7.76 (dd, *J* = 1.6, 0.6 Hz, 1H), 7.71 (s, 1H), 7.67 (d, *J* = 7.7 Hz, 1H), 7.56–7.52 (m, 2 H), 7.49–7.46 (m, 1H), 7.44–7.35 (m, 3 H), 7.09 (d, *J* = 3.1 Hz, 1H), 7.05–7.01 (m, 2 H), 6.52 (dd, *J* = 3.1, 0.6 Hz, 1H), 3.82 (s, 3 H), 2.43 (s, 3 H); $^{13}$C NMR (126 MHz, $CDCl_3$) δ 148.4, 141.8, 139.6, 136.5, 135.6, 135.1, 131.5, 129.9, 129.1, 129.0, 128.5, 125.9, 122.6, 121.3, 119.6, 109.7, 101.5, 33.1, 21.4; HRMS (ESI-TOF): m/z $[M+H]^+$ calcd $C_{22}H_{19}NO_3S$, 378.1159 for found 378.1162.

#### *4-(1-Methyl-1 H-indol-5-yl)phenyl 4-ethylbenzenesulfonate (1 m)*

Trituration was performed using diethyl ether and *n*-pentane(1:5) *v/v*; Yield: 56%; brown color solid; mp: 103–105 °C; $^1$H NMR (500 MHz, $CDCl_3$) δ 7.77 (dd, *J* = 8.9, 4.7 Hz, 3 H), 7.56–7.52 (m, 2 H), 7.42–7.33 (m, 4 H), 7.08 (t, *J* = 4.6 Hz, 1H), 7.05–7.01 (m, 2 H), 6.52 (d, *J* = 3.1 Hz, 1H), 3.82 (s, 3 H), 2.75 (q, *J* = 7.7 Hz, 2 H), 1.28 (t, *J* = 7.6 Hz, 3 H); $^{13}$C NMR (126 MHz, $CDCl_3$) δ 151.5, 148.4, 141.7, 136.5, 132.9, 131.5, 129.8, 129.1, 128.8, 128.7, 128.4, 122.6, 121.3, 119.6, 109.7, 101.5,33.1, 29.1, 15.1; HRMS (ESI-TOF): m/z $[M+H]^+$ calcd $C_{23}H_{21}NO_3S$, 392.1315 for found 392.1314.

**4-(1-Methyl-1 H-indol-5-yl)phenyl 4-methoxybenzenesulfonate (1n)** Trituration was performed using diethyl ether and *n*-pentane(1:5) *v/v*; Yield: 44%; brown color solid; mp: 116–118 °C; $^1$H NMR (500 MHz, $CDCl_3$) δ 7.82–7.75 (m, 3 H), 7.54 (d, *J* = 8.6 Hz, 2 H), 7.39 (dd, *J* = 17.0, 5.0 Hz, 2 H), 7.09 (d, *J* = 3.0 Hz, 1H), 7.03 (d, *J* = 8.6 Hz, 2 H), 6.98 (d, *J* = 8.9 Hz, 2 H), 6.52 (d, *J* = 2.9 Hz, 1H), 3.89 (s, 3 H), 3.82 (s, 3 H); $^{13}$C NMR (126 MHz, $CDCl_3$) δ 164.1, 148.3, 141.6, 136.4, 131.4, 130.9, 129.7, 129.0, 128.3, 126.9, 122.6, 121.2, 119.4, 114.3, 109.6, 101.4, 55.7, 33.0; HRMS (ESI-TOF): m/z $[M+H]^+$ calcd for $C_{22}H_{19}NO_4S$, 394.1108 found 394.1110.

**4-(1-Methyl-1 H-indol-5-yl)phenyl 3,4-dimethoxybenzenesulfonate (1o)** Trituration was performed using diethyl ether and *n*-pentane(1:5) *v/v*; Yield: 68%; off white color solid; mp: 137–139 °C; $^1$H NMR (500 MHz, $CDCl_3$) δ 7.76 (d, *J* = 1.0 Hz, 1H), 7.57–7.52 (m, 2 H), 7.46 (dd, *J* = 8.5, 2.1 Hz, 1H), 7.42–7.35 (m, 2 H), 7.27 (d, *J* = 2.1 Hz, 1H), 7.09 (d, *J* = 3.1 Hz, 1H), 7.06–7.01 (m, 2 H), 6.92 (d, *J* = 8.5 Hz, 1H), 6.52 (d, *J* = 3.0 Hz, 1H), 3.96 (s, 3 H), 3.86 (s, 3 H), 3.82 (s, 3 H); $^{13}$C NMR (126 MHz, $CDCl_3$) δ 153.9, 149.2, 148.5, 141.8, 136.5, 131.5, 129.9, 129.1, 128.4,126.9, 123.1, 122.7, 121.3, 119.6, 110.8, 110.5, 109.7, 101.5,77.4, 77.2, 76.9, 56.4, 56.4, 33.1; HRMS (ESI-TOF): m/z $[M+H]^+$ calcd for $C_{23}H_{21}NO_5S$, 424.1213 found 424.1219.

#### *General experimental procedure for the synthesis of indole sulfamate compounds (1p, 1q)*

To a stirred solution of compound **4** (40 mg, 0.18 mmol, 1.0 eq.) in DMAc (2 mL) added appropriate sulfamoyl chlorides (0.54 mmol, 3 eq.) at 0 °C under a nitrogen atmosphere over 10 min and then stirred at rt. After 2 h, the reaction was quenched using Sat. aq. $NaHCO_3$ solution and the obtained reaction mixture was continued to stir for an additional 1 h, then the resultant solid was filtered off and followed by triturated using diethyl ether and *n*-pentane to give required sulfamates **1p** and **1q** in good yields.

**4-(1-Methyl-1 H-indol-5-yl)phenyl sulfamate (1p)** Trituration was performed using diethyl ether and *n*-pentane(1:5) *v/v*; Yield: 56%; Green color solid; mp: 171–173 °C; $^1$H NMR (500 MHz, Acetone-$d_6$) δ 7.84 (s, 1H), 7.75–7.69 (m, 2 H), 7.51–7.45 (m, 2 H), 7.42–7.36 (m, 2 H), 7.27 (d, *J* = 3.1 Hz, 1H), 7.16 (s, 2 H), 6.50 (d, *J* = 3.0 Hz, 1H), 3.87 (s, 3 H); $^{13}$C NMR (126 MHz, Acetone-$d_6$) δ 150.5, 142.2, 137.7, 132.2, 131.2, 130.4, 129.1, 123.7, 121.8, 120.0, 111.0, 102.2, 33.2.; HRMS (ESI-TOF): m/z $[M+H]^+$ calcd for $C_{15}H_{14}N_2O_3S$, 303.0798 found 303.0799.

**4-(1-Methyl-1 H-indol-5-yl)phenyl methyl sulfamate (1q)** Trituration was performed using diethyl ether and *n*-pentane(1:5) *v/v*; Yield: 54%; Pale pink color solid; mp: 169–171 °C; $^1$H NMR (500 MHz, Acetone-$d_6$) δ 7.84 (s, 1H), 7.77–7.70 (m, 2 H), 7.51–7.45 (m, 2 H), 7.40–7.35 (m, 2 H), 7.27 (d, *J* = 3.1 Hz, 1H), 6.50 (d, *J* = 3.0 Hz, 1H), 3.87 (s, 3 H), 2.92 (s, 3 H); $^{13}$C NMR (126 MHz, Acetone-

$d_6$) δ 150.0, 142.1, 137.5, 131.9, 130.9, 130.2, 129.0, 123.2, 121.5, 119.8, 110.7, 101.9, 33.0, 30.3; HRMS (ESI-TOF): m/z $[M+H]^+$ calcd $C_{16}H_{16}N_2O_3S$, 317.0955 for found 317.0965.

#### *General process for the synthesis of target indole sulfamate compounds (1r-t)*

To a stirred solution of compound **4** (40 mg, 0.18 mmol, 1.0 eq.) in DMF (2 mL) added NaH (0.56 mmol, 2.5 eq.) at 0 °C and stirred for 20 min under $N_2$. Following this, added dropwise appropriate sulfamoyl chlorides (0.54 mmol, 3 eq.) in DMF (1 mL) at 0 °C under a nitrogen atmosphere over 10 min and then stirred at rt. After 2 h, the reaction was quenched with $H_2O$ (10 mL) and the obtained reaction mixture was partitioned between EtOAc (20 mL) and $H_2O$ (30 mL). Separated the organic layer and washed with sat. aq. NaCl solution (15 mL) and dried over anhydrous $Na_2SO_4$, filtered, and concentrated under reduced pressure. Further purification was carried out by trituration method using diethyl ether and *n*-pentane to afford the compounds **1r-t** in moderate (41–48%).

**4-(1-Methyl-1 H-indol-5-yl) phenyl dimethyl sulfamate (1r)** Trituration was performed using diethyl ether and *n*-pentane(1:5) *v/v*; Yield: 48%; pink color solid; mp: 147–149 °C; Yield:48%; $^1$H NMR (500 MHz, Acetone-$d_6$) δ 7.84 (s, 1H), 7.75 (d, *J* = 8.6 Hz, 2 H), 7.52–7.44 (m, 2 H), 7.39 (d, *J* = 8.6 Hz, 2 H), 7.27 (d, *J* = 3.0 Hz, 1H), 6.50 (d, *J* = 3.0 Hz, 1H), 3.87 (s, 3 H), 3.00 (s, 6 H); $^{13}$C NMR (126 MHz, Acetone-$d_6$) δ 149.1, 141.3, 136.6, 131.0, 130.0, 129.3, 128.2,, 122.1, 120.7, 119.0, 109.8, 101.0, 38.1, 32.1; HRMS (ESI-TOF): m/z $[M+H]^+$ calcd for $C_{17}H_{18}N_2O_3S$, 331.1111 found 331.1120.

***4-(1-Methyl-1 H-indol-5-yl) phenyl pyrrolidine-1-sulfonate ( 1s)*** Trituration was performed using diethyl ether and *n*-pentane(1:5) *v/v*; Yield: 42%; Pale brown color solid; mp: 170–172 °C; $^1$H NMR (500 MHz, Acetone-$d_6$) δ 7.84 (t, *J* = 1.2 Hz, 1H), 7.76–7.73 (m, 2 H), 7.48 (d, *J* = 1.1 Hz, 2 H), 7.42–7.38 (m, 2 H), 7.27 (d, *J* = 3.1 Hz, 1H), 6.50 (d, *J* = 3.1 Hz, 1H), 3.87 (s, 3 H), 3.46–3.41 (m, 4 H), 2.00–1.96 (m, 4 H); $^{13}$C NMR (126 MHz, Acetone-$d_6$) δ 150.1, 142.1, 137.5, 131.9, 130.9, 130.2, 129.0, 123.1, 121.6, 119.8, 110.7, 101.9, 50.0, 33.0, 26.3; HRMS (ESI-TOF): m/z $[M+H]^+$ calcd for $C_{19}H_{20}N_2O_3S$, 357.1268 found 357.1279.

**4-(1-Methyl-1 H-indol-5-yl) phenyl piperidine-1-sulfonate (1 t)** Trituration was performed using Diethyl ether and *n*-pentane (1: 5) *v/v*; Yield: 41%; brown color solid; mp: 138–140 °C; $^1$H NMR (500 MHz, $CDCl_3$) δ 7.80 (s, 1H), 7.64 (d, *J* = 7.0 Hz, 2 H), 7.51–7.29 (m, 4 H), 7.09 (s, 1H), 6.53 (s, 1H), 3.83 (s, 3 H), 3.50–3.34 (m, 4 H), 1.79–1.61 (m, 6 H); $^{13}$C NMR (126 MHz, $CDCl_3$) δ 149.1, 141.4, 136.5, 131.8, 129.8, 129.1, 128.6, 122.0, 121.4, 119.6, 109.7, 101.5, 48.1, 33.1, 25.2, 23.6; HRMS (ESI-TOF): m/z $[M+H]^+$ calcd for $C_{20}H_{22}N_2O_3S$, 371.1424 found 371.1436.

### In vitro urease inhibition assay

The urease inhibitory activity of the compounds **1a-t** was measured using a modified indophenol method [33, 34]. In 96-well plates, a mixture of 70 µL buffer pH 8.2 (0.01 mol/L $K_2HPO_4$, 100 mmol/L urea, 1 mmol/L EDTA and 0.01 mol/L $LiCl_2$), 10 µL urea substrate, 10 µL of 5 U/mL urease, and 10 µL of the test compounds (1 mM) were incubated for 5 min at room temperature. Subsequently, 10 µL of coloring agent (0.5% w/v NaOH, 0.1% active chloride NaOCl) was added to each well. After 10 min, the absorbance was measured at 630 nm using an ELISA plate reader. Data were collected in triplicate and the percentage of urease inhibition was calculated using the following formula:

% Inhibition = 100 − (O.D test compound/O.D control) ×100.

The $IC_{50}$ values were determined using non-linear regression analysis of concentration-response curves generated from at least triplicate experiments. Data was analyzed using a four-parameter logistic model in GraphPad Prism, which is the gold standard for enzymatic and pharmacological $IC_{50}$ determination.

### Antimicrobial activity screening against *H. pylori*, *E. coli* and Gut microflora

#### *Bacterial culture*

The *H. pylori* strain ATCC 43,504 (DSM 21031) was obtained from the German Collection of Microorganisms and Cell Cultures (DSMZ, Germany). It was cultured on Brucella agar (Sigma, USA) enriched with 10% horse serum and Skirrow Campylobacter Selective Supplement (Oxoid, UK), and incubated at 37 °C for 3–5 days under microaerophilic conditions (5% $O_2$, 10% $CO_2$, 85% $N_2$), generated using either CampyGen 2.5 L gas packs in anaerobic jars (BioMérieux, France) or a Whitley A20 Microaerophilic Workstation (Don Whitley, UK). The *Escherichia coli* ATCC 25,922 (ATCC, USA) was grown aerobically on MacConkey agar at 37 °C for 24 h. *Lactobacillus* strains, (*L. acidophilus*, *L. casei*, *L. gasseri*, *L. johnsonii*, *L. plantarum*, and *L. rhamnosus*) were sourced from Microbiologics (USA), cultivated on MRS agar (Sigma, USA), and incubated anaerobically for 24 h at 37 °C using 2.5 L AnaeroGen sachets (BioMérieux, France). Gram staining was periodically performed to verify strain purity and morphology. Following microbroth dilution assays, bacterial spotting and subsequent Gram staining were performed to confirm bacillary morphology and rule out contamination.

#### *Antibacterial Susceptibility Testing*

The antimicrobial susceptibility of *H. pylori* was assessed using the agar dilution method, following the CLSI 2024 guidelines to determine the minimum inhibitory concentration. The MIC was determined for each compound using a standardized broth microdilution method. Bacterial suspensions were adjusted to 2 McFarland standards ($1 \times 10^7$–$1 \times 10^8$ CFU/mL) using a DensiCHEK turbidimeter (BioMérieux, France). Aliquots (5 µL) were spot-inoculated onto Mueller-Hinton agar (Sigma, USA) supplemented with 10% horse serum (Sigma, USA) and Skirrow Campylobacter Selective Supplement (Oxoid, Thermo Scientific, UK). The agar plates were prepared with eight different concentrations [200 µM, 100 µM, 50 µM, 25 µM, 12.5 µM, 6.25 µM, 3.12 µM and 1.56 µM] of the tested compounds (1a-t). The MIC was defined as the lowest concentration at which complete bacterial growth inhibition was observed. A positive control consisted of *H. pylori* inoculated onto drug-free agar. For *E. coli*, a bacterial suspension of 0.5 McFarland ($1.5 \times 10^8$ CFU/mL) was prepared and tested against the two most promising compounds, 1 h and 1k, using the agar dilution method with the same concentration range [100 µM-0.098 µM]. To determine half-maximal inhibitory concentration ($IC_{50}$), a micro broth dilution assay was performed for the 20 compounds 1a-t using Mueller-Hinton broth (Sigma, USA) supplemented with 10% Horse serum (Sigma, USA) and Skirrow Campylobacter Selective Supplement (Oxoid, Thermo Scientific, UK). Two-fold serial dilutions of each compound were prepared in microtiter plates, ranging from 100 µM to 0.049 µM. An equal volume of *H. pylori* suspension (1.0 McFarland standard) was added to each well, followed by incubation at 37 °C under microaerophilic conditions. For *E. coli* and *Lactobacillus* strains, bacterial suspensions were prepared at a 0.5 McFarland standard using Mueller-Hinton broth and MRS broth, respectively. Optical density was measured at 570 nm using a Synergy H1 microplate reader (BioTek, USA) after 72 h of incubation for *H. pylori* and 24 h for *E. coli* and *Lactobacillus* species. $IC_{50}$ values were determined using GraphPad Prism version 10.4.2 (GraphPad Inc., La Jolla, CA, USA). All compounds were dissolved in dimethyl sulfoxide (DMSO; Sigma, USA) at a maximum concentration of 100 µM, with the final DMSO concentration not exceeding 2% (v/v). At this level, DMSO exhibited no inhibitory effects on *H. pylori*, ensuring that observed antimicrobial activity was attributable to the compounds. Amoxicillin (Sigma, USA) was used as the positive control at concentrations of 10 µg/mL and 0.007 µg/mL for *H. pylori*. Acetohydroxamic acid (AHA; Sigma, CAS No. 546-88-3) was employed as the positive control for anti-urease activity. Antimicrobial susceptibility testing was performed in triplicate using the agar dilution method and in duplicate using the microbroth dilution method for all 20 compounds. For compounds 1 h and 1k, four independent microbroth dilution assays were conducted to verify consistent activity.

### Cytotoxicity testing against human gastric epithelial cells and human dermal fibroblasts

#### *Mammalian cell culture*

Human gastric adenocarcinoma cells (AGS; ATCC CRL-1739 CLS, Germany) and normal fibroblast cells (F180) were cultured in RPMI-1640 (R8758-500ML, Sigma-Aldrich) and Dulbecco's Modified Eagles Medium (DMEM; D6429-500mL, Sigma-Aldrich), respectively. RPMI-1640 and DMEM were supplemented with 10% and 20% Fetal Bovine Serum (FBS; F2442-500ML, Sigma-Aldrich), respectively. Both media were further enriched with 1% penicillin-streptomycin (100 µg/mL and 100 IU/mL; P4333-100ML, Sigma-Aldrich). The cells were incubated at 37 °C in a humidified atmosphere with 5% $CO_2$ and cultured in polystyrene T75 (75cm$^2$) culture flasks (734–2313, VWR). Once the cultures attained 70–80% confluency, they were utilized for experimentation. Before subculturing or experimentation, cells were washed with Dulbecco phosphate buffered saline (PBS) (D8537-500ML, Sigma-Aldrich) and detached using a trypsin-EDTA solution (T4299-100ML, Sigma-Aldrich).

#### *MTT Cytotoxicity Assay*

The cytotoxicity of the two most promising compounds, 1 h and 1k, was evaluated using the 3-(4,5-Dimethyl-2-thiazolyl)–2,5-diphenyl-2 H-tetrazolium bromide (MTT) assay (M5655-1G, Sigma-Aldrich). AGS cells (4,500 cells per well) were seeded in 96-well plates (3599, Corning) and allowed to adhere and grow for 24 h before separate treatment with five different concentrations [6.25 µM, 3.125 µM, 1.5625 µM, 0.78 µM, and 0.39 µM] of each compound. Similarly, fibroblasts were seeded in 24-well plates (130186, ThermoScientific) at a density of 20,000 cells per well and subjected to the same treatment conditions It is noteworthy that the selected concentration range was designed to overlap with the previously determined minimum inhibitory concentration (MIC) values of 1 h and 1k against *H. pylori*, ensuring the relevance of cytotoxicity findings to their antibacterial potential.

Following 48-hour incubation, the medium was removed from each well and replaced with 100 µL of MTT solution (1:10 dilution; 500 µg/mL) per well for the 96-well plates and 200 µL per well for the 24-well plates. The plates were incubated at 37 °C for an additional 2 h. Following incubation, the MTT solution was discarded, having the formed formazan crystals dissolve in 100 µL of Dimethyl sulfoxide (DMSO; 20688, ThermoScientific) per well for the 96-well plates and 400 µL per well for the 24-well plates. From each well in the 24-well plate, 200 µL of the solution was transferred to a 96-well plate for

accurate absorbance measurement. For complete solubilization, plates were agitated on a plate shaker for 15 min prior to absorbance measurement at 570 nm (Synergy H1 microplate reader, BioTek). $IC_{50}$ values were calculated from duplicate experiments using GraphPad Prism 10.4.2 (GraphPad Inc., La Jolla). The data were analyzed by one-way ANOVA followed by Tukey's test wherein * denotes $P < 0.05$, ** denotes $P \leq 0.01$, *** denotes $P \leq 0.001$ and ns: non-significant difference.

### Urease activity assay

Enzyme activity assessments were performed using the Urease Microplate Assay Kit (Catalog Number MBS8305401, My BioSource, San Diego, USA), with all reagents and experimental preparations carried out according to the manufacturer's protocol. *H. pylori* suspensions, standardized to 0.5 McFarland density, were incubated under various conditions, including untreated (positive control), in the presence of two test compounds (1 h and 1k) individually at their MIC and $IC_{50}$ concentrations, and alongside the urease inhibitor (AHA), as determined through prior agar dilution and microtiter broth dilution assays. Urease enzymatic activity was determined by quantifying the release of ammonia, with one unit of activity is defined as the amount of enzyme required to produce 1 µmol of ammonia per minute. Absorbance was measured at 620 nm, with ammonia concentrations calculated using the equation: Urease activity % = (*H. pylori* activity with compounds/*H. pylori* activity without compounds) × 100. The urease activity of the positive control provided in the kit was designated as 100%, serving as the baseline reference for comparative analysis. The data were analyzed by one-way ANOVA followed by Tukey's test in GraphPad Prism version 10.4.2, wherein * denotes $P < 0.05$, ** denotes $P \leq 0.01$, *** denotes $P \leq 0.001$ and ns: non-significant difference.

### Caco-2 A-B permeability

We have conducted the same procedure reported in the literature [22] but using LC-UV detector. The most active anti-*H. pylori* compounds 1 h, 1j, 1k, and 1n, along with the reference drugs labetalol and propranolol, were assessed for their permeability across Caco-2 monolayers (apical-to-basolateral, A-B) at pH 6.5–7.4 and at their respective MIC values against *H. pylori*.

### Molecular modelling protocols

#### *Structure selection and preparation*

Molecular docking studies were conducted to investigate the potential interactions between the synthetic compounds and the urease enzyme. The three-dimensional structure of *H. pylori* urease (PDB ID: 6ZJA) [23, 35] and jack bean urease (PDB ID: 4GY7) [36] was obtained from the Protein Data Bank and served as the receptor for docking. Before initiating the docking, the protein structures were analyzed for any missing residues, which were modelled and corrected using PDBFixer, a structure refinement tool integrated within the Neurosnap platform. The corrected models were then used for docking analysis after removing the crystallographic water molecules beyond 5 Å from the active site and adding the polar hydrogen atoms. The protein was assigned the protonation state at physiological pH [37, 38].

#### *Ligand preparation*

The ligand structures were prepared using energy minimization applying MM2 force field using Chem3D software functionality of CambridgeSoft Ultra 12.0 (https://computing.ch.cam.ac.uk/software/chemdraw-and-chemoffice).

#### *Docking studies*

The interaction between the most potent urease inhibitors 1 h, 1k, 1 m, and 1n against the enzyme urease was investigated by DiffDock, which is part of the Neurosnap platform and applies a diffusion-based generative model [39]. Unlike conventional docking tools, DiffDock does not rely on the grid parameters for selecting the active pocket in the protein; instead, it infers the druggable binding site through learned protein-ligand structural correlation. The inhibitor structures were provided in the form of SMILES along with the protein receptor in PDB format. Docking was performed to produce 100 binding conformations for each ligand, which were subsequently ranked using a learned confidence-based scoring function to identify the best pose. The best docked poses were evaluated for interactions with the binding pocket residues using BIOVIA Discovery Studio 2021 [40]. Additionally, the docking protocol was validated by redocking of the co-crystalline ligands of the selected proteins using the same protocol as described above and the poses were visualized and superimposed for analysis in PyMOL.

#### *ADMET analysis*

The ADMET analysis was performed using an advanced freely accessible platform ADMETlab 3.0 [41, 42]. It provides physiochemical, medicinal, absorption, distribution, metabolism, excretion (ADME), and toxicity endpoints. It accepts SMILES of compounds as input and provides results in graphical and tabular form.

#### *Molecular Dynamics Simulation*

To investigate the conformational dynamics and structural stability of the *H. pylori* urease and Jack bean urease, simulations were conducted on both the apo forms and the ligand-bound complexes, specifically involving compounds 1 h and 1n. The structures employed were obtained from prior molecular docking studies and

refined as described in our previous work [23]. System preparation followed a rigorously validated protocol previously employed by researchers [43–45]. Protonation states of ionizable residues were assigned at physiological pH (7.4), using a combination of MolProbity [46], H + + web server [47], and manual evaluation to ensure chemical accuracy. Lysine and arginine residues were maintained in their protonated (cationic) forms, while aspartate and glutamate were treated as deprotonated (anionic). Histidine residues were modelled in their neutral states, singly protonated either at the $N_\delta$ or $N_\varepsilon$ position, depending on their hydrogen bonding environment and electrostatic context. Topology and coordinate files were generated using the LEaP module of AmberTools22 [48]. The proteins were modelled using the ff19SB force field [49], while ligand parameters were derived using the General AMBER Force Field 2 (GAFF2) [50]. Each system was immersed in a truncated octahedral box of "optimal" 3-charge, 4-point rigid water model (OPC) water molecules [51], with a buffer of at least 10 Å between the solute and the box boundaries. Counter-ions ($Na^+$) were added to neutralize the system, using parameters from Joung and Cheatham [52]. All molecular dynamics simulations were carried out using AMBER 22 [48]. Initial energy minimization was performed using 2000 steps of the steepest descent algorithm, with positional restraints (5.0 kcal $mol^{-1}$) applied to the heavy atoms of the protein, while allowing solvent molecules and ions to relax. Following minimization, systems were heated to 298.15 K over 400 ps under constant volume conditions (NVT ensemble), employing a Langevin thermostat [53] with a collision frequency of 5 $ps^{-1}$. Protein backbone atoms remained restrained during this phase using a force constant of 5.0 kcal $mol^{-1}$. Equilibration was subsequently conducted under constant pressure (NPT ensemble) for 1 ns using the Berendsen barostat [54], during which positional restraints on the protein backbone were gradually reduced and then removed. For production, three independent 100 ns NPT simulations were performed for each system, with distinct random seeds. A 2 fs integration time step was used, and the SHAKE algorithm was applied to constrain all bonds involving hydrogen atoms [55, 56]. Non-bonded interactions were truncated at 10 Å, and long-range electrostatics were computed using the Particle Mesh Ewald (PME) method with a 10 Å real-space cut-off [57, 58]. Simulation trajectories were saved at 100 ps intervals for post-processing. Analyses were conducted using CPPTRAJ and PYTRAJ [59], and further complemented by MDAnalysis [60]. Molecular visualization and structural inspection were carried out using VMD [61] and PyMOL (version 2.3.0, open-source) [62].

## Result and discussions

### Synthesis of the target compounds

The synthetic route employed to obtain the target compounds 1a-v is illustrated in Scheme 1. The synthesis commenced with a Suzuki-Miyaura cross-coupling between 5-bromo-1-methyl-1*H*-indole (2) and 4-(4,4,5,5-tetramethyl-1,3,2-dioxaborolan-2-yl) phenol (3), catalysed by [$PdCl_2$(dppf)] using $K_2CO_3$ as base, yielding key phenolic intermediate 4. Subsequent derivatization of intermediate 4 was achieved through sulfonylation with various sulfonyl chlorides ($Et_3N$ as base) to afford sulfonate derivatives 1a-o In the continued synthesis of further analogues, the phenolic intermediate was treated with sulfamoyl chlorides to afford sulfamate derivatives. Interestingly, the reaction proceeded very poorly when TEA or DIPEA were used as bases, resulting in significantly lower yields compared to the sulfonate derivatives. This reduced efficiency can be attributed to the lower electrophilicity of sulfamoyl chlorides relative to sulfonyl chlorides, arising from electron donation by the nitrogen substituent, which decreases the reactivity of the sulfur center toward nucleophilic substitution. Notably, the use of NaH as a strong base facilitated the reaction, affording sulfamate analogues 1**p**-**t** in moderate to good yields. The complete structural representation

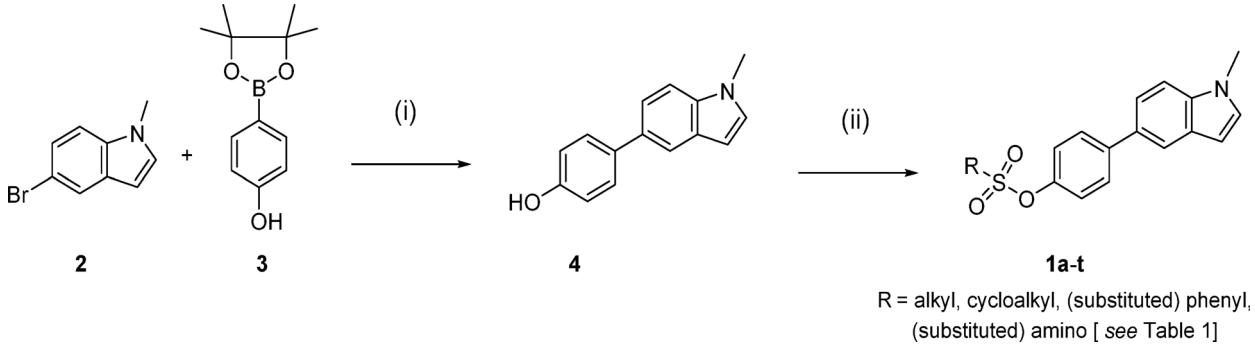


**Scheme 1** Reagents and conditions: (i) $K_2CO_3$, $PdCl_2$(dppf), $H_2O$, toluene, 95 °C, $N_2$, 8 h, 66%: (ii) appropriate sulfonyl chloride, TEA, DCM, 5–8 h, rt (1a-o: 47–91%); sulfamoyl chlorides or *N*-Me sulfamoyl chloride, anhydrous DMAc, rt, 2 h (1p: 56%, 1q: 54%); NaH, disubstituted sulfamoyl chlorides DMF rt, 2 h (1r: 48%, 1s: 42%, 1t: 41%)

and urease inhibitory activity data for all target indole derivatives are presented in Table 1.

## Biological activity of the target indole compounds

### *Urease inhibition*

This study sought to develop novel, potent urease inhibitors by designing fused heterocyclic compounds incorporating sulfonate and sulfamate moieties. The indophenol method was employed to evaluate the urease inhibitory activity of the synthesized compounds, using thiourea used as the standard inhibitor, exhibiting an $IC_{50}$ value of 23.2 ± 11.0 μM. All the urease inhibition assay were carried out in triplicate and each experiment was repeated thrice for reproducibility. As shown in Table 1, in vitro evaluation, eight compounds (1a, 1b, 1e, 1 g, 1 h, 1i, 1 m, and 1n) were identified as highly potent urease inhibitors with sub-micromolar $IC_{50}$ values (< 1 μM). Compounds 1c, 1j, 1k, 1 L, 1o, 1p, 1q, 1 s, and 1 t showed moderate activity ($IC_{50}$ = 1–10 μM), while 1f and 1r exhibited weak inhibition ($IC_{50}$ > 10 μM), and 1 d was the least active ($IC_{50}$ > 50 μM). Among the series, compound 1n (4-methoxy phenyl derivative) demonstrated an $IC_{50}$ value of 0.23 ± 0.33 μM, approximately 100-fold more potent than the standard inhibitor thiourea ($IC_{50}$ = 23.2 ± 11.0 μM In addition, compounds 1 m (4-Et-phenyl) and 1b (*n*-Pr) also demonstrated excellent potency with $IC_{50}$ values of 0.37 ± 0.001 μM and 0.39 ± 0.0003 μM, respectively, making both compounds around 63-fold and 59-fold respectively, more potent than the reference thiourea. The observed potency differences are rationalized by SAR and described in detail below.

Among the synthesized compounds, 1 m ($IC_{50}$ = 0.37 ± 0.001 μM) and 1n ($IC_{50}$ = 0.23 ± 0.03 μM) emerged as the most potent urease inhibitors. Both compounds possess extended conjugated systems in the form of ethyl benzene and methoxy benzene substituents. The presence of these moieties contributes to an optimal balance between aromaticity and spatial alignment for maximizing binding affinity. Other compounds containing electron donating groups (EDGs) also exhibited favorable inhibitory activities against urease. 1b ($IC_{50}$ = 0.39 ± 0.0003 μM) contains a propyl substituent, and 1e ($IC_{50}$ = 0.61 ± 0.0004 μM) has a cyclopropyl group. These groups enhance electron density around the sulfonate oxygen and promote favorable hydrogen bonding or van der Waals interactions with the active site residues. Additionally, 1a ($IC_{50}$ = 0.65 ± 0.002 μM), bearing an ethyl functional group, and 1 g ($IC_{50}$ = 0.72 ± 0.001 μM), with a benzyl substituent, were similarly potent.

In contrast, derivatives with electron withdrawing groups (EWGs) demonstrated moderately reduced activity. 1j ($IC_{50}$ = 5.78 ± 0.02 μM) and 1k ($IC_{50}$ = 1.39 ± 0.001 μM), bearing fluorobenzene and trifluoromethyl benzene groups respectively, exhibited a noticeable drop in potency relative to their EDGs-bearing analogues. Compounds substituted with bulky substituents displayed significantly lower activity, likely due to a combination of steric hindrance. 1 d ($IC_{50}$ = 50.14 ± 0.001 μM), which contains a butyl substituent, showed the weakest inhibition in the series. Similarly, 1f ($IC_{50}$ = 18.86 ± 0.15 μM), incorporating a cyclohexyl group, and 1r ($IC_{50}$ = 17.64 ± 0.04 μM), bearing a dimethylamine substituent, exhibited poor potency. The pyrrolidine-containing compound 1 s ($IC_{50}$ = 4.10 ± 0.007 μM) followed a similar trend. In a nutshell, electron donating, lipophilic, and spatially compact groups on the sulfonate moiety contribute positively to urease inhibitory activity by promoting optimal hydrophobic interactions and favourable electronic effects at the binding site. Substituents that are large tend to reduce activity due to steric hindrance.

### *Anti-Helicobacter pylori activity*

The anti-*H. pylori* activity of novel indole-derived sulfonate and sulfamate compounds was systematically evaluated. Both the minimum inhibitory concentration (MIC) and half-maximal inhibitory concentration ($IC_{50}$) values were determined and are depicted in Table 2.

All synthesized compounds 1a-t exhibited promising antibacterial activity against *H. pylori*. Several derivatives surpassed the activity of reference drug acetohydroxamic acid (MIC = 12,500 ± 2.08 μM; $IC_{50}$ = 7.38 ± 0.32 μM). Among them, compound 1k exhibited the highest potency with MIC < 1.5 μM and an $IC_{50}$ of 1.169 ± 0.03 μM. Other derivatives with significant activity included compound 1 h (MIC = 2.31 ± 1.145 μM; $IC_{50}$ = 2.058 ± 0.27 μM) and compound 1o (MIC = 4.685 ± 2.213 μM; $IC_{50}$ = 0.65 ± 0.60 μM). Additionally, compounds 1j, 1n, and 1 m also demonstrated low MIC and $IC_{50}$ values, indicating strong inhibitory potential. These findings highlight the strong antibacterial potential of the series, particularly compounds 1 h and 1k as lead candidates for further investigation as evidenced by their lowest MIC and $IC_{50}$ values. The justification for the noticed potency differences based on SARs is described in detail below.

The SAR analysis of compounds 1a-t against *H. pylori* demonstrated that increasing the hydrophobicity and steric bulk of the sulfonate substituent generally enhanced antibacterial activity. Among the alkyl-substituted derivatives, activity improved from ethyl (1a, MIC = 100 μM) to *n*-propyl derivative 1b (MIC = 12.5 μM), while the branched isomer 1c (MIC = 25 μM) exhibited reduced potency, suggesting a preference for linear alkyl chains. The *n*-butyl sulfonated compound, 1 d, displayed comparable activity to compound 1b, indicating that further chain extension does not necessarily translate to enhanced efficacy. Within the cycloalkyl series, cyclohexyl derivative 1f demonstrated superior activity compared to cyclopropyl sulfonated compound

**Table 1** Urease inhibitory potency of the target *N*-methyl Indole scaffolds 1a-t

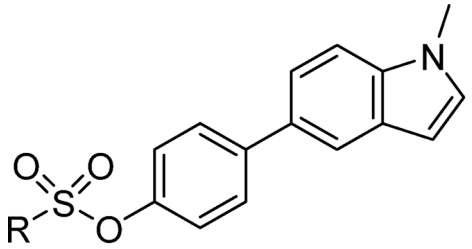


| Compound No | R | $IC_{50}$± SEM (μM)*/ % inhibition |
|---|---|---|
| **1a** | Et | 0.65 ± 0.002 |
| **1b** | *n*-Pr | 0.39 ± 0.0003 |
| **1c** | 2-Pr | 2.95 ± 0.03 |
| **1d** | Bu | 50.14 ± 0.001 |
| **1e** | Cyclopropyl | 0.61 ± 0.0004 |
| **1f** | Cyclohexyl | 18.86 ± 0.15 |
| **1g** | Ph | 0.72 ± 0.001 |
| **1h** | 4-Tolyl | 0.95 ± 0.001 |
| **1i** | *4-tert*-Bu-$C_6H_4$ | 0.46 ± 0.002 |
| **1j** | 4-F-$C_6H_4$ | 5.78 ± 0.02 |
| **1k** | 4-$(CF_3)C_6H_4$ | 1.39 ± 0.001 |
| **1L** | 3-Tolyl | 1.57 ± 0.003 |
| **1m** | 4-Et-$C_6H_4$ | 0.37 ± 0.001 |
| **1n** | 4-OMe-$C_6H_4$ | 0.23 ± 0.033 |
| **1o** | 3,4-$(OMe)_2$-$C_6H_3$ | 1.57 ± 0.03 |
| **1p** | $NH_2$ | 1.44 ± 0.001 |
| **1q** | NHMe | 6.58 ± 0.007 |
| **1r** | $NMe_2$ | 17.64 ± 0.04 |
| **1s** | pyrrolidinyl | 4.10 ± 0.007 |
| **1t** | piperidinyl | 1.60 ± 0.003 |
| **Thiourea** | | 23.2 ± 11.0 |

*The $IC_{50}$ values are expressed as means of triplicate assays ±SEM

**Table 2** Evaluation of the anti-*Helicobacter pylori* activity of *N*-methylindole sulfonate and sulfamate compounds 1a-t, alongside the acetohydroxamic acid (AHA), against *H. pylori*

| Compounds | MIC value against H. pylori ± SD (μM) * | $IC_{50}$ value against H. pylori ± SD (μM) |
|---|---|---|
| **1a** | 100 | 15.2 ± 5.70 |
| **1b** | 12.5 | 10.5 ± 0.46 |
| **1c** | 25 | 8.82 ± 1.0 |
| **1d** | 12.5 | 7.77 ± 0.14 |
| **1e** | 18.75 ± 8.838 | 9.23 ± 2.11 |
| **1f** | 12.5 | 5.20 ± 2.71 |
| **1 g** | 12.5 | 7.79 ± 0.80 |
| **1 h** | 2.31 ± 1.145 | 2.058 ± 0.27 |
| **1i** | 12.5 | 8.90 ± 1.48 |
| **1j** | 4.685 ± 2.213 | 3.69 ± 0.12 |
| **1k** | < 1.5 | 1.169 ± 0.03 |
| **1 L** | 9.375 ± 4.419 | 5.12 ± 1.03 |
| **1 m** | 4.7 ± 2.192 | 4.26 ± 1.14 |
| **1n** | 6.25 | 2.16 ± 0.19 |
| **1o** | 4.685 ± 2.213 | 0.65 ± 0.60 |
| **1p** | 75 ± 35.35 | 3.54 ± 0.38 |
| **1q** | 37.5 ± 17.67 | 9.95 ± 6.29 |
| **1r** | 37.5 ± 17.67 | 7.39 ± 2.11 |
| **1s** | 18.75 ± 8.838 | 7.23 ± 3.01 |
| **1t** | 56.25 ± 61.87 | 6.74 ± 2.87 |
| **AHA** | 12,500 ± 2.08 | 7.38 ± 0.320 |

* MICs are reported as mean values of triplicate determinations ± standard deviation (SD), while $IC_{50}$ represent mean values of duplicate assays ± SD

1e, supporting the role of increased hydrophobic volume in improving target interaction. Introduction of aromatic substituents led to a marked improvement in potency, the phenyl derivative 1 g was further enhanced by *para*-substituted electron-donating or hydrophobic groups, as observed in compounds 1 h (4-$CH_3$-) and 1 m (4-$CH_2CH_3$Ph-). Notably, the 4-trifluoromethyl derivative 1k emerged as the most potent compound (MIC < 1.5 μM), while the *meta*-substituted analogue 1 L was significantly less active, indicating a clear preference for *para* substitution. Electron-donating methoxy groups (1n, 1o) moderately enhanced activity. In contrast, amino-substituted derivatives (1p–r) exhibited weaker activity, potentially due to increased polarity and reduced membrane permeability. Among cyclic amines, pyrrolidine sulfonated compound 1 s, was more effective than piperidine derivative 1 t, suggesting that smaller, more rigid ring systems may offer improved compatibility with the bacterial target. Structure–activity relationship analysis showed that both electronic and steric factors were involved in inhibitory effect against urease when the synthesized indole-based sulfonate and sulfamate derivatives were evaluated. In general, compounds with aromatic sulfonate moiety electron-donating substituents showed increased urease inhibitory activity. In line with the observed activity trends, it is projected that increased π-electron density favor stabilizing aromatic and electrostatic interactions within the urease active site. Inhibitory potency was also affected by substituent size and spatial orientation. The catalytic cavity was able to accommodate moderately sized aromatic substituents, while increased steric bulk resulted in decreased activity, probably because of less-than-ideal placement in relation to the dinuclear nickel center. When compared to sulfonate analogues, sulfamate derivatives generally showed somewhat lower inhibitory activity. This could be due to variations in polarity and hydrogen-bonding geometry within the active site.

A concise SAR summary and the most potent hits against urease and *H. pylori* are presented in Fig. 4.

### *Cytotoxicity Assay*

The cytotoxic potential of compounds 1 h and 1k, the most potent anti-*H. pylori* derivatives, was evaluated against AGS gastric adenocarcinoma cells and F180 normal fibroblasts (Fig. 5). Cell viability was assessed using the MTT assay, and results are expressed as survival fractions relative to untreated controls. Both compounds exhibited minimal cytotoxicity against AGS cells at concentrations up to 6.25 μM, with 1k showing a slightly greater, but statistically insignificant reduction in cell viability. In contrast, neither compound showed appreciable cytotoxicity toward F180 cells, with $IC_{50}$ values exceeding

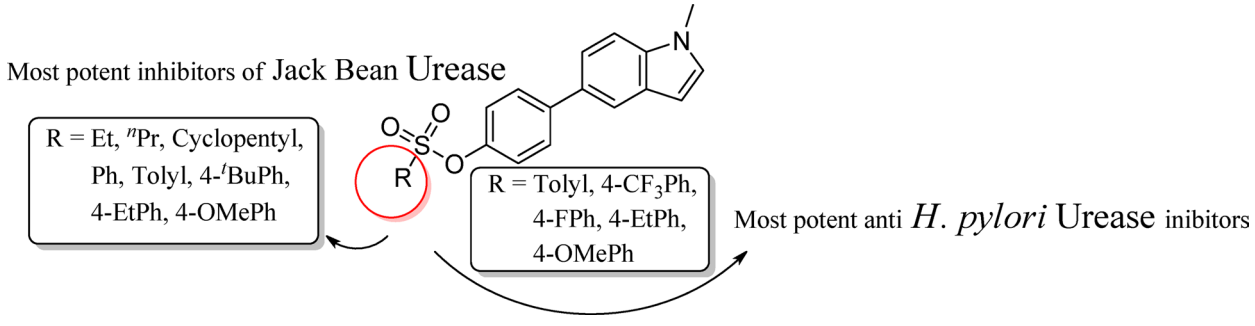


**Fig. 4** SAR highlights and top-performing anti-urease compounds against jack-bean and *H. pylori* urease

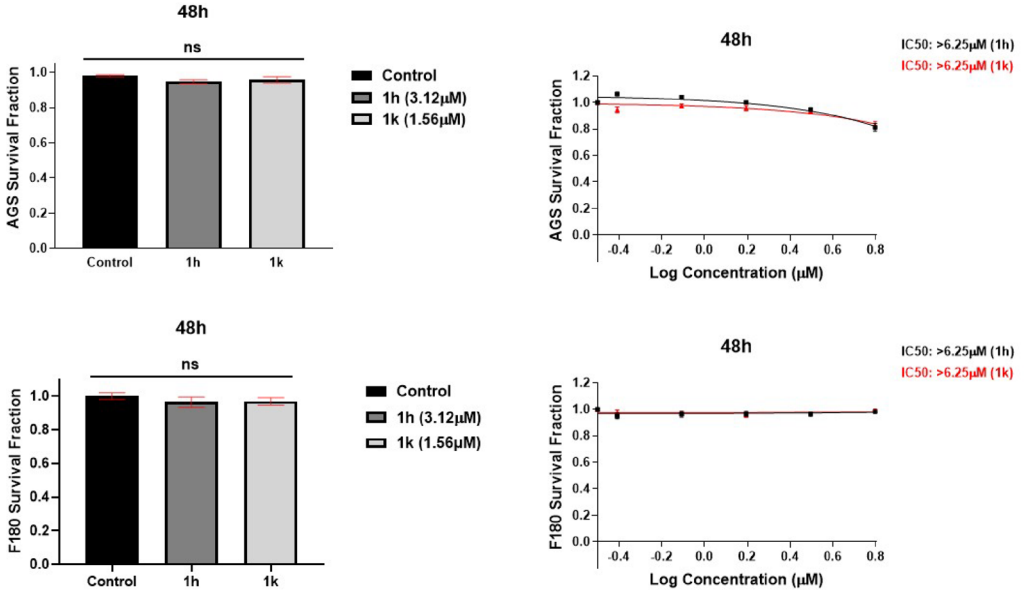


**Fig. 5** Cytotoxic effect of 1 h (3.12μM) and 1k (1.56μM) on AGS gastric cancer cells (top left) and F180 normal fibroblasts (bottom left) after 48 h of treatment. Dose-response curves depicting the cytotoxicity of 1 h (black) and 1k (red) in AGS (top right) and F180 (bottom right) following 48 h of treatment. Statistical values were obtained using the one-way ANOVA followed by Tukey's test, executed in GraphPad Prism 10.4.2. ns: non-significant difference

**Table 3** Selectivity of compounds 1 h, 1k and AHA against urease positive (*H. pylori*) and urease negative (*E. coli*)

| Compounds | MIC value against H. pylori ± SD (μM) * | $IC_{50}$ value against H. pylori ± SD (μM) * | MIC value against E. coli ± SD (μM) * | $IC_{50}$ value against E. coli ± SD (μM) * |
|---|---|---|---|---|
| **1 h** | < 0.78 | 4.05 ± 0.25 | > 20 | No effect |
| **1k** | < 0.78 | 1.97 ± 0.07 | > 20 | No effect |
| **AHA** | 12,500 ± 2.08 | 7.3 ± 0.32 | - | - |

*The MICs and $IC_{50}$s calculated as a means of two independent experiments ± SD

6.25 μM for 1 h and 1k. The survival fraction of AGS and F180 cells following 48 h treatment with 1 h (3.12 μM) and 1k (1.56 μM) remained above 90% for both cell lines. These results indicate that 1 h and 1k exhibit minimal cytotoxicity at their MICs toward the tested cell lines, supporting their favorable safety profiles and potential for further development as selective anti-*H. pylori* agents.

### *Urease activity assessment of the most promising compounds against H. pylori, E. coli and Lactobacillus species*

To evaluate the selectivity of the *N*-methylindole derivatives 1 h and 1k toward urease-producing bacteria, their inhibitory activities were compared against both urease-negative (*E. coli*) and urease-positive (*H. pylori*) strains (Tables 3 and 4). The findings revealed that both compounds exhibited no inhibitory effect on *E. coli*, whereas a significant suppression of *H. pylori* was observed. This selective inhibition suggests that the tested compounds specifically target urease-positive bacteria, with a pronounced effect on *H. pylori*. Further evaluation against several *Lactobacillus* species (*L. acidophilus*, *L. casei*, *L. gasseri*, *L. johnsonii*, *L. plantarum*, and *L. rhamnosus*) demonstrated no significant growth inhibition, suggesting minimal off-target effects on beneficial commensal microbes. Collectively, these findings highlight the selective antimicrobial activity of the tested compounds against *H. pylori* while preserving the commensal microbial balance, distinguishing them from broad-spectrum antibiotic treatments.

### *Inhibition of H. pylori urease activity by 1 h and 1k*

The results of the urease activity assay, as shown in Fig. 6, demonstrate a strong significant inhibitory effect of both test compounds, 1 h and 1k, on *H. pylori* urease activity. Compared to the untreated *H. pylori* control, treatment with 1 h and 1k at MIC resulted in a marked reduction in activity to below 20%. When tested at their $IC_{50}$ concentrations, both compounds maintained a moderate inhibitory effect, with residual urease activities ranging between 43% and 48%, indicating dose-dependent inhibition. The reference positive control inhibitor (AHA), reduced urease activity to baseline, confirming assay sensitivity. Importantly, no urease activity was detected in non-*H. pylori* controls, including *E. coli* and *L. acidophilus*, validating the assay specificity for *H. pylori* urease. These findings suggest that both 1 h and 1k effectively

**Table 4** Selectivity of compounds **1 h**, **1k** and AHA against L. acidophilus, L. casei, L. gasseri, L. johnsonii, L. plantarum, and L. rhamnosus

| Compounds | MIC value against L. acidophilus ± SD (μM) * | $IC_{50}$ value against L. acidophilus ± SD (μM) * | MIC value against L. casei ± SD (μM) * | $IC_{50}$ value against L. casei ± SD (μM) * |
|---|---|---|---|---|
| **1 h** | > 20 | No effect | > 20 | No effect |
| **1k** | > 20 | No effect | > 20 | No effect |
| **AHA** | > 20 | 12.25 ± 0.37 | > 20 | No effect |
| **Compounds** | **MIC value against *L. gasseri* ± SD (μM) *** | **$IC_{50}$value against *L. gasseri* ± SD (μM) *** | **MIC value against*L. johnsonii* ± SD (μM) *** | **$IC_{50}$value against *L. johnsonii* ± SD (μM) *** |
| **1k** | > 20 | No effect | > 20 | No effect |
| **1 h** | > 20 | No effect | > 20 | No effect |
| **AHA** | > 20 | 23.35 ± 0.82 | > 20 | 37.12 ± 0.44 |
| **Compounds** | **MIC value against *L. plantarum* ± SD (μM) *** | **$IC_{50}$value against *L. plantarum* ± SD (μM) *** | **MIC value against *L. rhamnosus* ± SD (μM) *** | **$IC_{50}$value against *L. rhamnosus* ± SD (μM) *** |
| **1 h** | > 20 | No effect | > 20 | No effect |
| **1k** | > 20 | No effect | > 20 | No effect |
| **AHA** | > 20 | No effect | > 20 | 56.18 ± 0.41 |

*The MICs and $IC_{50}$s were calculated as a means of two independent experiments ± SD

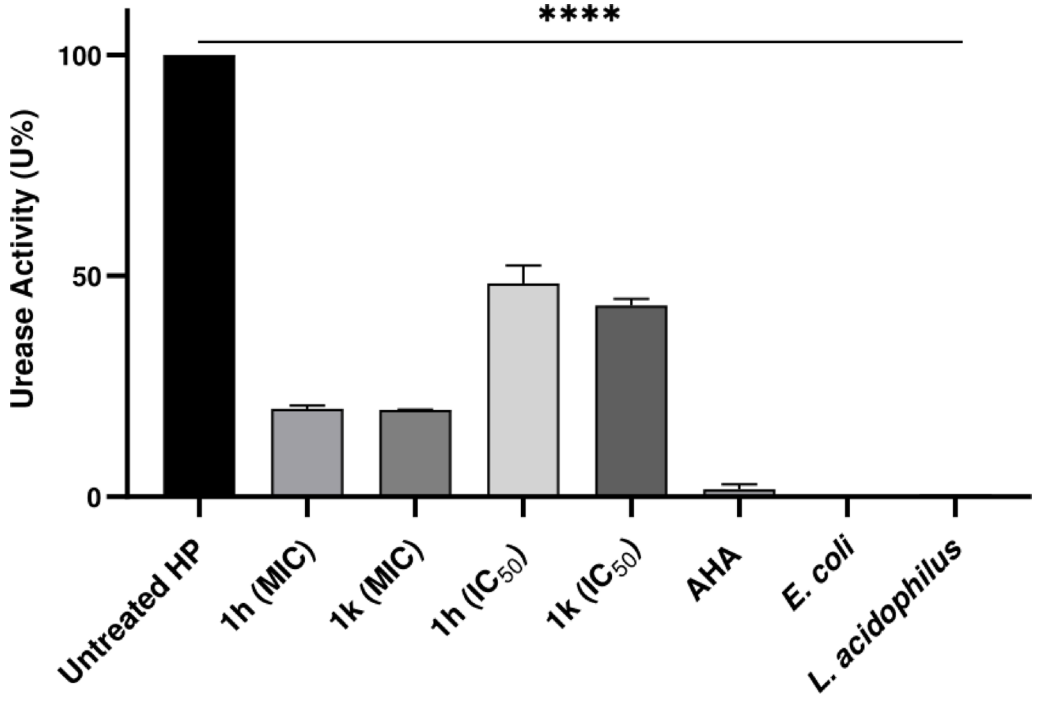


**Fig. 6** Assessment of *H. pylori* urease activity following exposure to selected *N*-methylindole derivative compounds 1 h and 1k at their respective MIC and $IC_{50}$ concentrations, alongside AHA as a reference indicator. Data are presented as mean ± SD from two independent experiments, and the urease activity (%) was determined using the equation: U % = (Urease activity with compounds/Urease activity without compounds) × 100. Data were as analyzed using one-way ANOVA followed by Tukey's post hoc test (****$P \leq 0.0001$)

suppress *H. pylori* urease activity, particularly at bacteriostatic concentrations.

### *Caco-2 A-B permeability*

The Caco-2 permeability assay is commonly used to evaluate the potential oral absorption of test compounds [63]. Herein, the most active anti-*H. pylori* compounds 1 h, 1j, 1k, and 1n, along with the reference drugs labetalol and propranolol, were assessed for their permeability across Caco-2 monolayers (apical-to-basolateral, A-B) at pH 6.5–7.4 and at their respective MIC values against *H. pylori*. The results are summarized in Table 5.

The four tested compounds exhibited very low permeability, suggesting minimal oral absorption (Table 5). This

**Table 5** Caco-2 A-B permeability of the most active anti-helicobacter compounds and the reference drugs labetalol and propranolol at pH 6.5–7.4.5.4[a]

| Tested compound | Test concentration (μM) | Permeability ($10^{-6}$ cm/s)[a] | % Recovery |
|---|---|---|---|
| **1 h** | 2.31 | 0.008 ± 0.001 | 12.10% ± 0.15% |
| **1j** | 4.685 | 0.013 ± 0.0005 | 11.48% ± 0.13% |
| **1k** | 1.5 | 0.006 ± 0.0007 | 4.65% ± 0.08% |
| **1n** | 6.25 | 0.004 ± 0.0004 | 23.34% ± 0.31% |
| **Labetalol** | 10 | 3.94 ± 0.11 | 68.65% ± 0.24% |
| **Propranolol** | 10 | 33.08 ± 0.52 | 92.39% ± 0.45% |

[a] The results are expressed as means of triplicate experiments ± SEM

is a significant finding, as it implies that these compounds may primarily exert their activity within the gastrointestinal tract (GIT) without substantial systemic exposure, potentially reducing the risk of systemic side effects At present, no direct assessments of the stability of these compounds in the GIT have been conducted. Nonetheless, further chemical and metabolic studies evaluating their stability under gastrointestinal conditions would be highly relevant and would strengthen the interpretation of the present findings.

### *Molecular docking analysis*

To investigate the binding potential and conformational stability of the most active urease inhibitors 1 h and 1k against *H. pylori* urease along with 1 m and 1n against jack bean urease, molecular docking was performed using DiffDock.

Docking simulations for 1 h revealed a DiffDock confidence score of −1.43, an indicative of a reliable pose prediction within the catalytic pocket of *H. pylori* urease. Its binding free energy was calculated to be −7.42 kcal/mol. The SMINA-based evaluation further provided a predicted affinity of −3.67 kcal/mol, an intramolecular energy of −0.94 kcal/mol and the post-minimization root-mean-square deviation (RMSD) was 1.17 Å. Compound 1k exhibited a DiffDock confidence score of −0.95, with a refined binding affinity of −7.12 kcal/mol. Its SMINA-derived affinity and intramolecular energy were 0.42 and − 0.95 kcal/mol, respectively, with an RMSD of 0.76 Å after minimization. On the other hand, AHA docked against urease showed a binding affinity of −1.63 kcal/mol with a DiffDock confidence score of 0.42. The minimized complex had a low root-mean-square deviation (RMSD) of 0.49 Å and an intramolecular binding energy of −2.62 kcal/mol.

For 1 m, the docking analysis disclosed a DiffDock confidence score of −1.6, which is an indicative of a reliable predicted pose within the jack bean urease active site. The binding affinity, calculated after refinement was − 4.81 kcal/mol and SMINA-derived affinity and intramolecular energy values were 0.70 and − 1.00 kcal/mol, respectively. The RMSD after minimization was 1.17 Å, indicating low deviation from the initial pose. Compound 1n, on the other hand, showed a confident DiffDock score of −1.3 and a minimized binding affinity of −4.87 kcal/mol, implying a somewhat stronger ligand-receptor interaction. The associated affinity and intramolecular energy values were − 0.86 and − 0.95 kcal/mol, respectively, while the post-minimization RMSD was observed to be 1.47 Å. The binding energies observed for both ligands fall within the pharmacologically relevant range [64], comparable to established urease inhibitors. Apart, thiourea displayed a binding free energy of −1.66 kcal/mol and a DiffDock confidence score of 0.41. An intramolecular energy of −2.20 kcal/mol with a post-minimization RMSD of 0.64 Å was obtained by SMINA rescoring.

Besides, the docking protocol was validated by redocking of co-crystalline ligands of 6zja (*H. pylori* urease) and 4gy7 (jack bean urease). In case of *H. pylori* urease, the docked complex of 6zja and 2-{[1-(3,5-dimethylphenyl)−1*H*-imidazol-2-yl]sulfanyl}-N-hydroxyacetamide (DJM) have binding free energy of −6.15 kcal/mol with a diffdock confidence score of −0.17. It occupied the same place as of co-crystalline ligand in the 6zja retrieved from RCSB PDB with an RMSD of 0.001 Å as shown in Fig. 7A. Likewise, the redocked complex of jack bean urease (4gy7) and it co-crystalline ligand (phosphate) exhibited a binding energy of −2.69 kcal/mol with a diffdock confidence score of 0.24. This docked pose was then superimposed with the 4gyr retrieved from RCSB PDB and it was disclosed that the binding site of both the phosphate as shown in Fig. 7B.

**Intermolecular interactions** The docking analysis of the compound 1 h within the active site of *H. pylori* urease revealed stabilizing molecular interactions (Fig. 8A). Three conventional hydrogen bonds were formed, involving the carbonyl oxygen atoms of the ligand and the side chains of THR251 and ARG338, with bond distances of approximately 2.93, 2.96 and 2.90 Å. These interactions are likely to play a pivotal role in anchoring the ligand within the catalytic domain of the enzyme. Additionally, a carbon–hydrogen bond was established between GLY280 and the ligand at a distance of 3.10 Å. The aromatic system of 1 h exhibited amide-π stacking interactions with ASN168, measured at 4.83 and 4.62 Å respectively, while also engaging in hydrophobic π-alkyl contacts with ALA169, LEU252, and CYS321, all within favorable van der Waals distances. Notably, π-sulphur interactions were observed between the ligand and HIS248 (4.87 Å) as well as HIS322 (5.68 Å). Moreover, a π-anion interaction with GLU222 at a distance of 3.80 Å was identified, suggesting an additional electrostatic contribution to ligand binding.

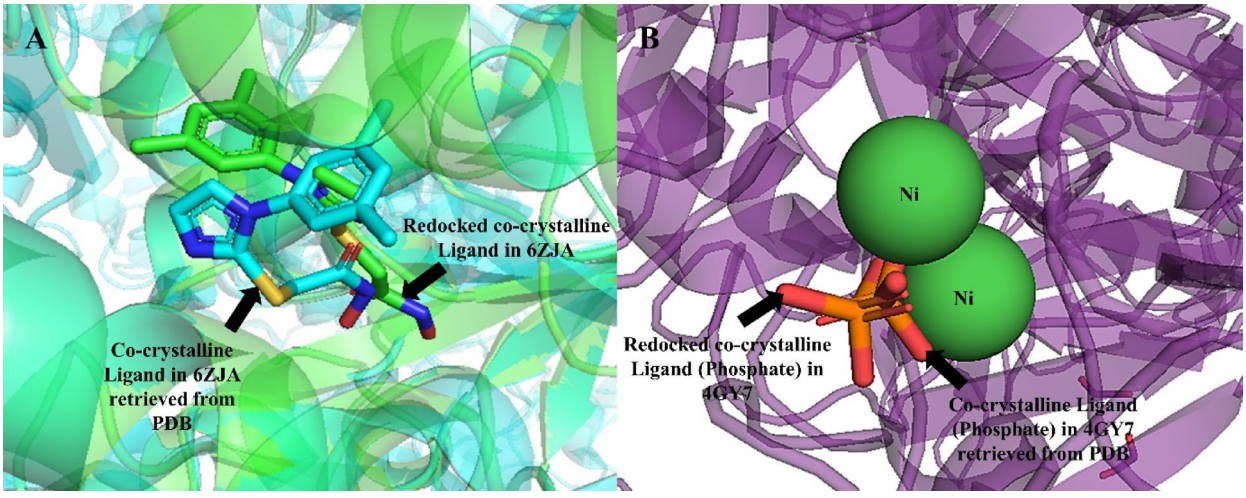


**Fig. 7** **(A)** Superimposed redocked complex (green) and protein retrieved from PDB (blue) for *H. pylori* urease. **(B)** Superimposed redocked complex and protein retrieved from PDB for jack bean urease

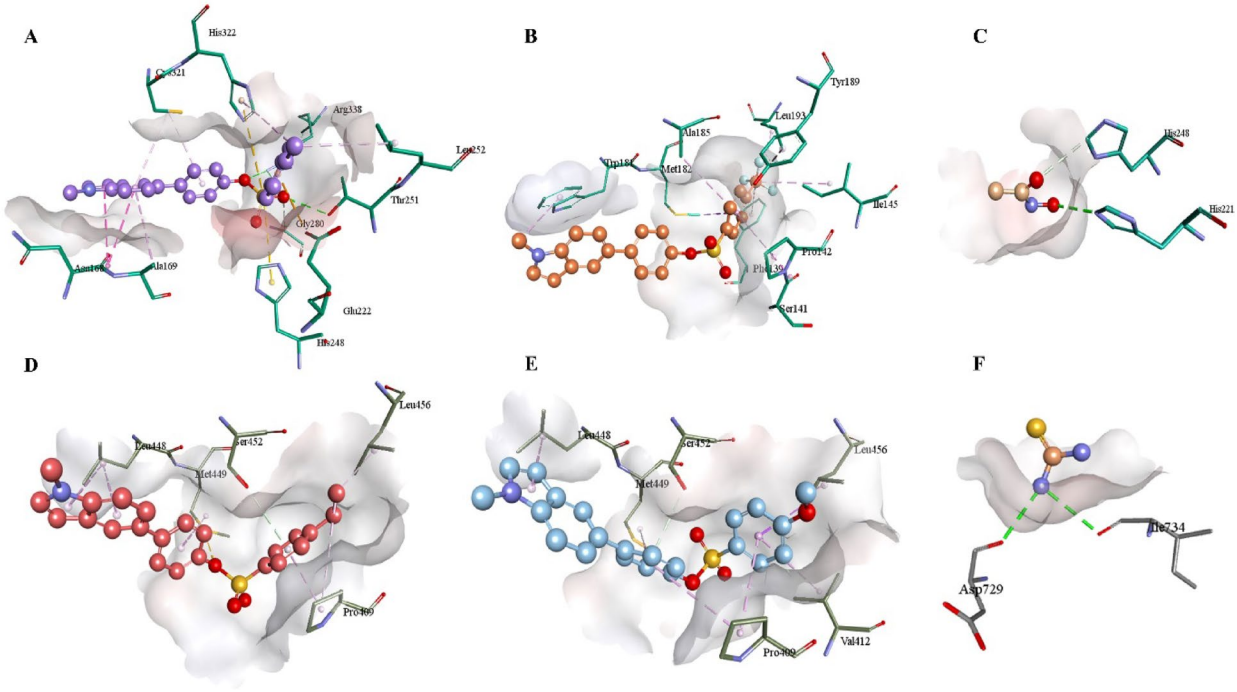


**Fig. 8** Intermolecular interactions of potent inhibitors **1 h (A)**, 1k **(B)**,AHA **(C)** docked against *H. pylori* urease (green sticks), and 1 m **(D)**, 1n **(E)**,thiourea **(F)** docked against jack bean urease (grey sticks)

The docking study of compound 1k within the binding site of *H. pylori* urease demonstrated several important intermolecular interactions (Fig. 8B). The amino acid residues TYR189, SER141, TRP181, MET182, and PRO142 were identified as key contributors to ligand binding, with measured distances consistent with specific non-covalent interactions. PHE139, ILE145, TYR189 and LEU193 showed interactions with electron deficient carbon of substituted trifluoromethyl group of 1k. SER141 engaged the ligand at distance of 5.17 Å. In addition, MET182 developed π-sigma interaction. TRP181 formed π-alkyl bond with the terminal methyl group with a distance of 4.22 Å.

AHA forms a conventional hydrogen bond with HIS221, involving the hydroxamate oxygen atom of AHA and the imidazole side chain of histidine, at a distance of 3.10 Å (Fig. 8C). In addition, a carbon-hydrogen bond interaction is observed between AHA and HIS248, with an interaction distance of 3.62 Å. Although weaker than conventional hydrogen bonds, carbon-hydrogen

interactions can contribute cumulatively to ligand stabilization.

The intermolecular interaction evaluation of 1 m disclosed a combination of hydrophobic, hydrogen bond, and sulfur-related interactions (Fig. 7D). A notable interaction was identified between the sulfonyl group of the ligand and the sulfur atom of MET449, resulting in a sulfur oxygen contact with 2.78 Å bond length. This interaction namely sulfur-X type is significant in stabilizing ligand-protein complexes, due to their polarizability and favorable dispersion forces. Further a π-donor hydrogen bond interaction between an aromatic moiety of the ligand and SER452 (3.87 Å) was observed. 1 m also formed hydrophobic interactions, particularly with nonpolar residues such as LEU456 (3.28 Å), LEU448 (4.81 and 4.97 Å), and PRO409 (3.44 and 5.30 Å). These mainly involve alkyl and π-alkyl interactions contributing to the desolvation of the active site and increase the entropic favorability of binding. The π-alkyl interaction between the aromatic ring of the ligand and MET449 (5.18 Å) also stabilizes the complex and enhances the ligand stability within the hydrophobic core of the enzyme.

The compound 1n is embedded in a hydrophobic cavity formed by LEU456, LEU448, MET449, PRO409, VAL412, and SER452 in active site of urease where all play vital roles in anchoring and stabilizing the ligand (Fig. 7E). An interaction involves the aromatic ring of the ligand forming a π-donor hydrogen bond interaction with SER452 at a distance of 3.64 Å. Besides, several π-alkyl and π-sigma interactions were also identified, contributing to hydrophobic stabilization of 1n. The aromatic ring adjacent to the sulfonyl group forms a π-sigma interaction with LEU456 (3.00 Å). Furthermore, π-alkyl interactions with PRO409 (4.45 Å), VAL412 (5.18 Å), MET449 (5.17 Å), and LEU448 (5.21 Å) contributes to the compound's secure fit within the hydrophobic pocket.

Thiourea forms two conventional hydrogen bonds interactions, highlighted by green dashed lines as in Fig. 8F. One hydrogen bond is established between the amino nitrogen of thiourea and the backbone carbonyl oxygen of ILE734, with an interaction distance of 3.35 Å. A second, stronger hydrogen bond is observed between thiourea and ASP729, with a bond distance of 2.98 Å. The type of interactions for all the discussed compounds have been elucidated in Table 6 to better apprehend.

### *ADMET analysis*

The pharmacokinetic and toxicological characteristics of the synthesized compounds 1 h, 1k, 1 m, and 1n were investigated using the ADMETlab 3.0 platform as summarized in Table S2 and Fig. 9. Each compound followed Lipinski's Rule of Five and met the Golden Triangle criterion, indicating promising oral bioavailability and balanced molecular properties. Importantly, none of the compounds raised Pan-Assay Interference Compounds (PAINS) alerts, thereby reducing the risk of non-specific biological activity.

The compounds showed poor predicted human intestinal absorption, with probability values below 0.01.

The distribution characteristics suggested that these compounds would primarily remain within the vascular and interstitial compartments, as indicated by their low predicted volumes of distribution (–0.26 to 0.32 L/kg). Blood-brain barrier (BBB) penetration was limited in most cases, though 1k exhibited the highest probability of central nervous system access (0.25). This restricted CNS permeability may be beneficial in avoiding neurological side effects.

Metabolic profiling revealed strong inhibitory interactions with several cytochrome P450 enzymes, particularly CYP2C19, CYP2C9, CYP2D6, and CYP3A4, with probabilities exceeding 0.89. Substrate potential varied

**Table 6** The type of interactions exhibited by the potent compounds upon docking within *H. pylori* and jack bean urease

| Compounds | Lipophilic interactions | | Polar interactions | | Hydrogen bond interactions | |
|---|---|---|---|---|---|---|
| | Amino acids | Interaction type | Amino acids | Interaction type | Amino acids | Interaction type |
| **1 h** | LEU252, ALA169, CYS321, ASN168 | Alkyl, π-alkyl | GLU222, HIS248, HIS322 | π-anion, π-sulfur, amide-π stacked | THR251, ARG338, GLY280 | H-bond, C-H bond |
| **1k** | TRP181, TYR189, PHE139, PRO142, ILE145, LEU193 | | SER141; MET182 | π-sigma, amide-π stacked | None observed | |
| **Acetohydroxamic acid (AHA)** | None observed | | None observed | | HIS221; HIS248 | H-bond, C-H bond |
| **1 m** | PRO409, LEU448, LEU456 | | MET449 | π-sulfur | SER452 | H-bond |
| **1n** | PRO409, LEU448, MET449, LEU456 | | LEU456 | π-sigma | SER452 | π-donor hydrogen bond |
| **Thiourea** | None observed | | None observed | | ILE734; ASP729 | H-bond |

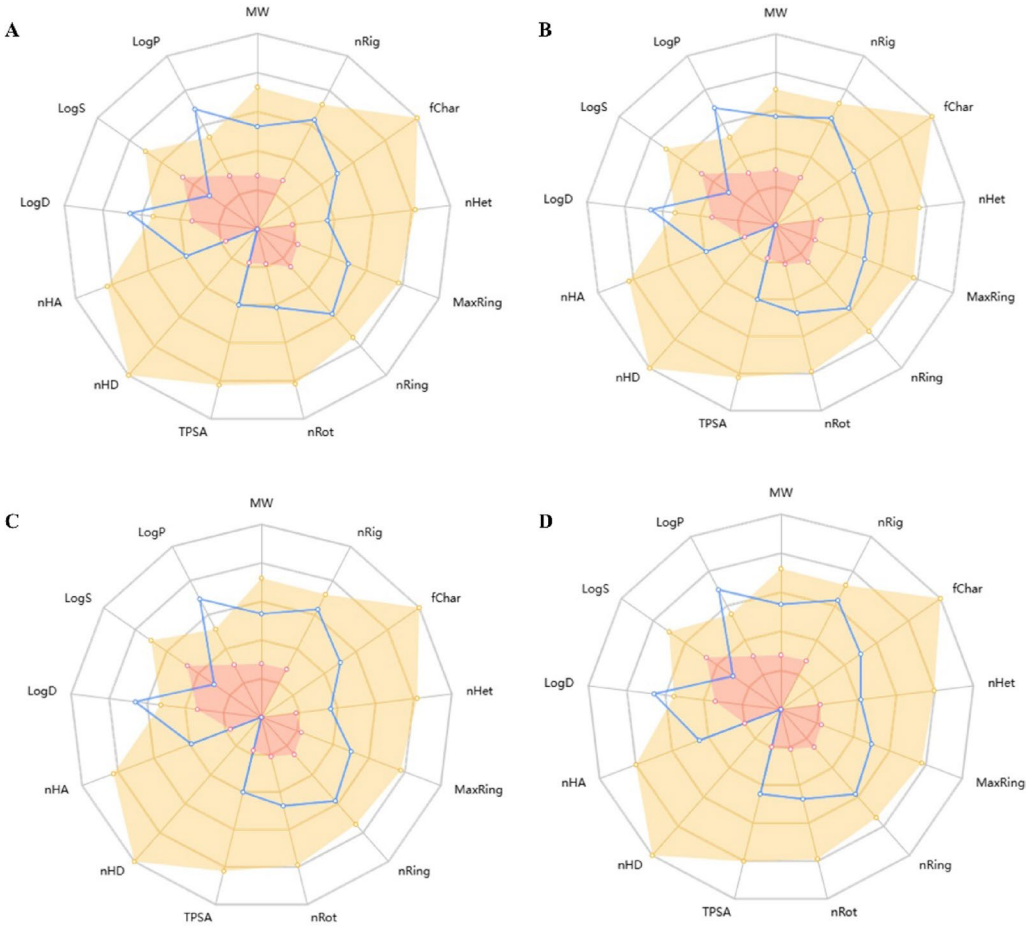


**Fig. 9** The radar charts elucidating the physiochemical properties of potent inhibitors 1 h **(A)**,1k **(B)**, 1 m **(C)** and 1n **(D).** The blue lines are representing the properties of respective compounds while the red colored region is indicating the lower acceptable limit and the orange color region is representing the upper acceptable limit

across enzymes, with 1 m exhibiting a high likelihood of being metabolized by CYP3A4 (probability: 0.97).

Regarding elimination, the predicted clearance ranged from 3.43 to 4.73 mL/min/kg, accompanied by short elimination half-lives (0.38 to 0.44 h), suggesting rapid systemic clearance.

Toxicological evaluation showed no indications of acute toxicity, genotoxic or non-genotoxic carcinogenicity, or ocular corrosiveness. All four compounds were predicted to inhibit the hERG potassium channel with moderate probabilities (0.57–0.66), suggesting a potential cardiotoxicity risk that would require in vitro validation through electrophysiological assays. Additionally, all compounds were identified as potential inducers of drug-induced liver injury (DILI) that may hinder long-term administration.

The likelihood of mutagenicity, assessed via Ames test modelling, varied among the compounds, with 1k showing the lowest risk (0.13) and 1n the highest (0.56), necessitating further experimental confirmation. Predicted carcinogenic potential was particularly notable for 1n (0.82), representing the need for thorough long-term safety evaluation. Furthermore, all molecules displayed strong binding affinities (0.98–0.99) to estrogen receptors, indicating possible endocrine-disrupting effects. Mitochondrial membrane potential disruption was predicted with high confidence (0.93–0.98). Activation of the antioxidant response element and the aryl hydrocarbon receptor by these compounds suggests their involvement in oxidative stress regulation and xenobiotic response pathways.

### *Molecular Dynamics Simulation*

A 100-nanosecond molecular dynamics simulation was carried out to investigate the stability and conformational changes of *H. pylori* urease bound to the inhibitor 1 h. Three key parameters were examined: backbone root-mean-square deviation (RMSD), radius of gyration (Rg), and root-mean-square fluctuation (RMSF) of individual residues. The RMSD values for both the free *H. pylori* urease and bound complex are shown in Fig. 10A. The unbound urease structure exhibited larger fluctuations

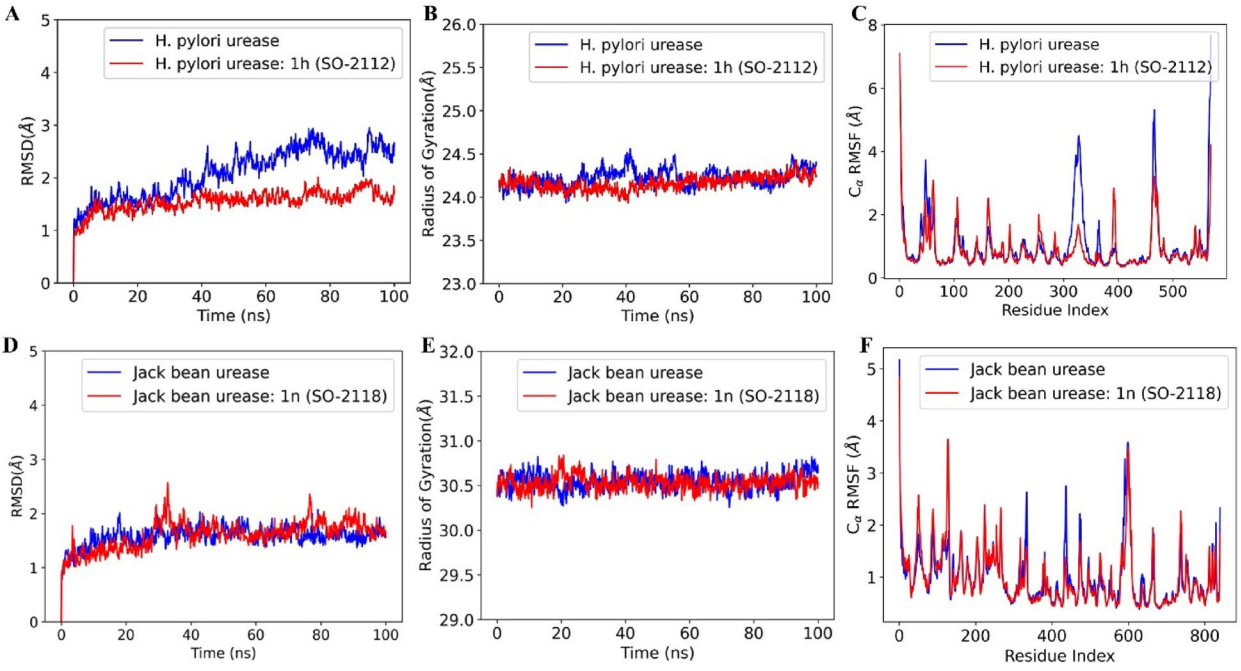


**Fig. 10** RMSD **(A)**, radius of gyration **(B)** and RMSF **(C)** plots for *H. pylori* urease in apo form (blue) and bound to 1 h (red) over 100 ns of simulation. RMSD **(D)**, radius of gyration **(E)** and RMSF **(F)** plots for Jack bean urease in apo form (blue) and bound to 1n (red) over 100 ns of simulation

during the simulation, with RMSD values ranging from 1.0 Å to 3.0 Å and stabilized near 2.7 Å after 60 ns. In contrast, the complex with 1 h showed smaller deviations, reaching a stable RMSD around 1.6 Å after 40 ns.

Figure 10B illustrates the per-residue fluctuations of the Cα atoms throughout the simulation period. The apo-*H. pylori* urease structure displayed higher flexibility in certain loop and terminal regions, especially between residues 1–30, 60–90, around 320, and near residue 490. When **1 h** was bound, these fluctuations were reduced. The lower RMSF values in key regions of the protein imply that the ligand contributes to stabilizing the active site and nearby structural elements, thereby reducing local mobility.

The radius of gyration analysis (Fig. 10C) was used to analyze changes in the overall compactness of the protein. Both forms of urease (apo and ligand bound) showed relatively consistent Rg values during the 100 ns simulation. However, the ligand bound form maintained slightly lower Rg values (approximately 24.1–24.3 Å), indicating a more compact structure in the presence of the ligand. This reduced flexibility and increased compactness showed enhanced stability of the enzyme upon ligand interaction.

To assess the structural stability and dynamic behaviour of Jack bean urease upon ligand interaction, molecular dynamics (MD) simulations were conducted for both the unbound enzyme and its complex with 1n. The RMSD profile indicated that both systems achieved equilibrium within the simulation timeframe (Fig. 10D). The apo urease was stabilized after approximately 15–20 ns, maintaining an average RMSD of 1.6 Å. The urease-1n complex exhibited a similar trend, albeit with slightly elevated fluctuations during the early phase of the simulation (0–25 ns), likely corresponding to initial conformational accommodation of the ligand within the binding cavity. The average RMSD of the complex over the final 75 ns was approximately 1.7 Å, reflecting a well-stabilized ligand-bound state. Minor deviations observed during the analysis, particularly around 30–40 ns and near 80 ns, remained within acceptable limits and did not indicate any unfolding or loss of structural integrity. The marginal increase in RMSD in the complex relative to the apo structure is consistent with the dynamic adaptation.

The Rg values are crucial for determining the overall compactness of the protein during simulation (Fig. 10E). The apo urease exhibited an average Rg of 30.55 Å, consistent throughout the trajectory. Upon ligand binding, the Rg of the complex decreased slightly to an average of 30.50 Å, suggesting a modest compaction of the enzyme tertiary structure. This minor decrease is indicative of stabilizing interactions induced by the ligand within the binding pocket, which may contribute to enhanced rigidity, and local ordering around the active site. The absence of significant Rg fluctuations in either system indicates that the global fold of urease was preserved in both apo and bound states.

Residue-level flexibility was analyzed through root mean square fluctuation (RMSF) of Cα atoms over the course of the simulation. As illustrated in Fig. 10F, the

RMSF profiles revealed characteristic fluctuations across the protein chain for both systems. The apo enzyme exhibited notable mobility at the *N*- and *C*-terminal regions. Upon binding of 1n, a general trend of reduced fluctuation was observed in several regions, particularly between residues 100–150, 300–350, and 580–620, suggesting localized stabilization imparted by ligand interaction. Certain segments displayed increased flexibility in the ligand-bound complex, such as regions spanning residues 50–80 and 200–220. These changes may reflect ligand-induced conformational adjustments or allosteric effects, potentially facilitating optimal binding accommodation or altering distant dynamic regions of the protein.

The MDS for best docked complex of 1k has been illustrated in supplementary file.

## Conclusion

In this study, we successfully designed and synthesized a series of novel fused heterocyclic compounds, with the aim of identifying potent urease inhibitors. The biological evaluation of these compounds showed that several indole derivatives displayed significant in vitro urease inhibitory activity. The most potent compound, 1n, exhibited an $IC_{50}$ of $0.23 \pm 0.33$ µM, approximately 100-fold more potent than the standard thiourea, while 1b, 1 h, and 1 m also showed $IC_{50}$ values below 0.5 µM. SAR analysis indicated that small, linear alkyl chains and para-substituted electron-donating aryl substituents, enhanced urease-inhibitory activity, whereas steric hindrance and electron-withdrawing substituents reduced potency. The compounds also demonstrated selective antibacterial activity against *H. pylori*, with several compounds, particularly 1 h and 1k showing superior efficacy compared to the reference drug acetohydroxamic acid. These compounds exhibited minimal cytotoxicity toward AGS gastric and F180 normal fibroblast cell lines and did not inhibit *E. coli* or beneficial *Lactobacillus* species, highlighting their specificity for urease-positive pathogens. Urease activity assays confirmed a marked decrease in *H. pylori* urease activity following treatment with 1 h and 1k. Molecular docking studies of 1 h, 1k, 1 m, and 1n against *H. pylori* and Jack bean ureases revealed key stabilizing interactions. In *H. pylori* urease, residues THR251, ARG338, GLY280, ASN168, ALA169, LEU252, CYS321, HIS248, HIS322, GLU222, TYR189, SER141, TRP181, MET182, PRO142, PHE139, ILE145, and LEU193 contributed to binding, while in Jack bean urease, interactions involved MET449, SER452, LEU456, LEU448, PRO409, and VAL412. These interactions corroborate with the strong binding affinity and in vitro potency.

Compounds 1 h, 1k, 1 m, and 1n demonstrate promising drug-like properties and molecular suitability for lead development. However, their limited absorption, potential for metabolic inhibition, and predicted toxicities warrant cautious interpretation and further refinement. Overall, the research finds novel, selective, and potent urease enzyme inhibitors with promising antibacterial profiles, providing strong leads for the development of targeted therapies against urease-associated infections such as *H. pylori*.

## Supplementary Information

The online version contains supplementary material available at https://doi.org/10.1186/s13099-026-00814-8.

Supplementary Material 1

### Acknowledgements

The authors are thankful to the University of Sharjah, United Arab Emirates, for funding this study (grant #24011101106 & 24011101109 & 24011102102).

### Author contributions

G.K.: Conceptualization, Funding acquisition, Project administration, Supervision, Data curation, Investigation, Writing – original draft, Writing – review & editing, Validation. E.M.M.: Investigation, Methodology, Writing – original draft, Writing – review & editing, Validation. S.Z.: Conceptualization, Project administration, Supervision, Data curation, Investigation, Writing – original draft, Writing – review & editing, Validation. A.R.: Visualization, Investigation, Writing – original draft, Writing – review & editing. A.I.S.: Visualization, Investigation, Writing – original draft, Writing – review & editing. S.-O.Z.: Supervision, Investigation, Writing – review & editing. N.R.: Investigation, Methodology, Writing – original draft, Writing – review & editing, Validation. H.S.Anbar: Conceptualization, Visualization, Investigation, Methodology, Writing – original draft, Writing – review & editing, Validation. H.S.Ali: Investigation, Methodology, Writing – original draft, Writing – review & editing, Validation. S.Q.: Investigation, Methodology, Writing – original draft, Writing – review & editing, Visualization. M.S.: Investigation, Methodology, Writing – original draft. R.A.Z.: Investigation, Methodology, Writing – original draft, Writing – review & editing. M.I.E.: Conceptualization, Funding acquisition, Project administration, Supervision, Writing – review & editing, Validation, Visualization, Investigation.

### Funding

This research was funded by the competitive research grants [24011101106; 24011101109; 24011102102] from the University of Sharjah, United Arab Emirates.

### Data availability

No datasets were generated or analysed during the current study.

## Declarations

### Competing interests

The authors declare no competing interests.

### Author details

[1]Research Institute for Medical and Health Sciences, University of Sharjah, Sharjah 27272, United Arab Emirates
[2]Department of Pharmaceutics and Pharmaceutical Technology, College of Pharmacy, University of Sharjah, Sharjah 27272, United Arab Emirates
[3]Department of Basic and Applied Chemistry, Faculty of Science and Technology, University of Central Punjab, Lahore 54590, Pakistan
[4]Department of Pharmaceutical Sciences, College of Pharmacy, Dubai Medical University, Dubai 19099, United Arab Emirates
[5]Chemistry Research Laboratory, Department of Chemistry and the INEOS Oxford Institute for Antimicrobial Research, University of Oxford, 12 Mansfield Road, Oxford OX1 3TA, UK
[6]Department of Medicinal Chemistry, College of Pharmacy, University of Sharjah, Sharjah 27272, United Arab Emirates

[7]Department of Medicinal Chemistry, Faculty of Pharmacy, Mansoura University, Mansoura 35516, Egypt

**Received: 18 November 2025 / Accepted: 12 February 2026**
Published online: 04 March 2026

**References**

1. Collins CM, D'Orazio SEF. Bacterial ureases: structure, regulation of expression and role in pathogenesis. Mol Microbiol. 1993;9:907–13. https://doi.org/10.1111/j.1365-2958.1993.tb01220.x.
2. Mobley HLT. The role of *Helicobacter pylori* urease in the pathogenesis of gastritis and peptic ulceration. Aliment Pharmacol Ther. 1996;10:57–64. https://doi.org/10.1046/j.1365-2036.1996.22164006.x.
3. Rutherford JC. The emerging role of urease as a general microbial virulence factor. PLoS Pathog. 2014;10:e1004062. https://doi.org/10.1371/journal.ppat.1004062.
4. Boer JL, Mulrooney SB, Hausinger RP. Nickel-dependent metalloenzymes. Arch Biochem Biophys. 2014;544:142–52. https://doi.org/10.1016/j.abb.2013.09.002.
5. Konieczna I, Zarnowiec P, Kwinkowski M, Kolesinska B, Fraczyk J, Kaminski Z, et al. Bacterial urease and its role in long-lasting human diseases. Curr Protein Pept Sci. 2013;13:789–806. https://doi.org/10.2174/138920312804871094.
6. Burne RA, Chen YYM. Bacterial ureases in infectious diseases. Microbes Infect. 2000;2:533–42. https://doi.org/10.1016/S1286-4579(00)00312-9.
7. Scott DR, Marcus EA, Weeks DL, Sachs G. Mechanisms of acid resistance due to the urease system of *Helicobacter pylori*. Gastroenterology. 2002;123:187–95. https://doi.org/10.1053/gast.2002.34218.
8. Sachs G, Weeks DL, Melchers K, Scott DR. The gastric biology of *Helicobacter pylori*. Annu Rev Physiol. 2003;65:349–69. https://doi.org/10.1146/annurev.physiol.65.092101.142156.
9. Almarmouri C, El-Gamal MI, Haider M, Hamad M, Qumar S, Sebastian M, et al. Anti-urease therapy: a targeted approach to mitigating antibiotic resistance in *Helicobacter pylori* while preserving the gut microflora. Gut Pathog. 2025;17:37. https://doi.org/10.1186/s13099-025-00708-1.
10. Wang S, Lee MH, Hausinger RP, Clark PA, Wilcox DE, Scott RA. Structure of the dinuclear active site of urease. X-ray absorption spectroscopic study of native and 2-mercaptoethanol-inhibited bacterial and plant enzymes. Inorg Chem. 1994;33:1589–93. https://doi.org/10.1021/ic00086a006.
11. Park IS, Hausinger RP. Requirement of carbon dioxide for in vitro assembly of the urease nickel metallocenter. Science. 1995;267:1156–8. https://doi.org/10.1126/science.7855593.
12. Carter EL, Flugga N, Boer JL, Mulrooney SB, Hausinger RP. Interplay of metal ions and urease. Metallomics. 2009;1:207–21. https://doi.org/10.1039/b903311d.
13. De Reuse H, Vinella D, Cavazza C. Common themes and unique proteins for the uptake and trafficking of nickel, a metal essential for the virulence of *Helicobacter pylori*. Front Cell Infect Microbiol. 2013;3:72334. https://doi.org/10.3389/fcimb.2013.00094.
14. Nim YS, Wong KB. The maturation pathway of nickel urease. Inorganics. 2019;7:154. https://doi.org/10.3390/inorganics7070085.
15. Fong YH, Wong HC, Yuen MH, Lau PH, Chen YW, Wong KB. Structure of UreG/UreF/UreH complex reveals how urease accessory proteins facilitate maturation of *Helicobacter pylori* urease. PLoS Biol. 2013;11:e1001678. https://doi.org/10.1371/journal.pbio.1001678.
16. Goldie J, van Veldhuyzen Zanten SJO, Jalali S, Richardson H, Hunt RH. Inhibition of urease activity but not growth of *Helicobacter pylori* by acetohydroxamic acid. J Clin Pathol. 1991;44:695–7. https://doi.org/10.1136/jcp.44.8.695.
17. Itumoh EJ, Data S, Leitao EM. Opening up the toolbox: synthesis and mechanisms of phosphoramidates. Molecules. 2020;25:3684. https://doi.org/10.3390/molecules25163684.
18. Sharma A, Suhas R, Gowda DC. Ureas/thioureas of benzo[d]isothiazole analog conjugated glutamic acid: synthesis and biological evaluation. Arch Pharm. 2013;346:359–66. https://doi.org/10.1002/ardp.201200470.
19. Khan Y, Solangi M, Khan KM, Ullah N, Iqbal J, Hussain Z, et al. Exploration of thiazine Schiff bases as promising urease inhibitors: design, synthesis, enzyme inhibition, kinetic analysis, ADME/T evaluation, and molecular docking studies. Int J Biol Macromol. 2024;281:136361. https://doi.org/10.1016/j.ijbiomac.2024.136361.
20. Asadi GS, Abdizadeh R, Abdizadeh T. Investigation of a set of flavonoid compounds as *Helicobacter pylori* urease inhibitors: insights from in silico studies. J Biomol Struct Dyn. 2023;43:2366–88. https://doi.org/10.1080/07391102.2023.2295973.
21. Modolo L, de Souza AX, ivia L, Horta P, ebora D, Araujo P. An overview on the potential of natural products as ureases inhibitors: a review. J Adv Res. 2015;6:35–44. https://doi.org/10.1016/j.jare.2014.09.001.
22. Shahin AI, Zaib S, Zaraei S-O, Kedia RA, Anbar HS, Younas MT, et al. Design and synthesis of novel anti-urease imidazothiazole derivatives with promising antibacterial activity against *Helicobacter pylori*. PLoS One. 2023;18:e0286684. https://doi.org/10.1371/journal.pone.0286684.
23. Hashem O, Zaib S, Zaraei S-O, Javed H, Kedia RA, Anbar HS, et al. Design and discovery of urease and *Helicobacter pylori* inhibitors based on benzofuran/benzothiophene-sulfonate and sulfamate scaffolds for the treatment of ureolytic bacterial infections. Int J Biol Macromol. 2024;271:132502. https://doi.org/10.1016/j.ijbiomac.2024.132502.
24. Kalatuwawege IP, Gunaratna MJ, Udukala DN. Synthesis, in silico studies, and evaluation of syn and anti isomers of N-substituted indole-3-carbaldehyde oxime derivatives as urease inhibitors against *Helicobacter pylori*. Molecules. 2021;26:6658. https://doi.org/10.3390/molecules26216658.
25. Wang Y, Dang X, Zhang J, Tong H, Tang W, Liu B. Molecular docking and molecular dynamics simulations of the urease inhibitory activity of 2,3-dihydroxybenzohydrazide derivatives. ChemSelect. 2024;9:e202401432. https://doi.org/10.1002/slct.202401432.
26. Zaraei SO, El-Gamal MI, Shafique Z, Amjad ST, Afridi S, Zaib S, Anbar HS, El-Gamal R, Iqbal J. Sulfonate and sulfamate derivatives possessing benzofuran or benzothiophene nucleus as potent carbonic anhydrase II/IX/XII inhibitors. Bioorg Med Chem. 2019;27:3889–901. https://doi.org/10.1016/j.bmc.2019.07.026.
27. Jalil S, Ullah S, Zaraei SO, Sbenati RM, Shahin AI, AlKubaisi BO, et al. Synthesis and biological evaluation of sulfamate derivatives as inhibitors of carbonic anhydrases II and IX. Med Chem Res. 2023;32:869–83. https://doi.org/10.1007/s00044-023-03043-9.
28. Anbar HS, El-Gamal R, Ullah S, Zaraei SO, Al-Rashida M, Zaib S, Pelletier J, S\' evigny J, Iqbal J, El-Gamal MI. Evaluation of sulfonate and sulfamate derivatives possessing benzofuran or benzothiophene nucleus as inhibitors of nucleotide pyrophosphatases/phosphodiesterases and anticancer agents. Bioorg Chem. 2020;104:1–11. https://doi.org/10.1016/j.bioorg.2020.104305.
29. Rehman W, Khan Y, Farghaly TA, Sarfraz H, Arooj K, Naseem M. Synthesis and computational studies on novel thiazine-thiazole hybrid analogues as dual α-amylase and α-glucosidase inhibitors for combating diabetes mellitus. Comput Biol Chem. 2026;120:108786. https://doi.org/10.1016/j.compbiolchem.2025.108786.
30. Khan Y, Naeem MU, Arooj K, Naseem M, Adnan R, Azmatullah. A comprehensive computational and experimental study of novel imidazole linked thiadiazole based amide derivatives as cholinesterase duel-target inhibitor for the treatment of Alzheimer's disease. Comput Biol Chem. 2026;120:108789. https://doi.org/10.1016/j.compbiolchem.2025.108789.
31. Khan Y, Hussain R, Maqsood S, Naeem MU, da Araújo Costa R, Sattar A, et al. Design, synthesis and computational approaches of highly potent thiazole-based isoxazole targeting thymidine phosphorylase and urease inhibitors. Journal of Computational Biophysics and Chemistry. 2026;1:1–28. https://doi.org/10.1142/S2737416526500067.
32. Arshad S, Maalik A, Rehman W, Khan Y, Rasheed L, Alanazi AS, et al. Novel hybrid indazole-based 2,4-dihydro-3*H*-1,2,4-triazole-3-thione derivatives: design, synthesis, spectroscopic characterization, SAR, molecular docking, pharmacokinetics and toxicological activities. Pure Appl Chem. 2025;97:1923–46. https://doi.org/10.1515/pac-2025-0459.
33. Hina S, Zaib S, Uroos M, Zia-Ur-Rehman M, Munir R, Riaz H, et al. N-arylacetamide derivatives of methyl 1,2-benzothiazine-3-carboxylate as potential drug candidates for urease inhibition. R Soc Open Sci. 2023;10:230104. https://doi.org/10.1098/rsos.230104.
34. Khan Y, Hussain R, Rehman W, Khan S, Maalik A, Iqbal T, et al. *In-vitro* and *in-silico* assessment of thiazole-thiazolidinone derivatives as selective inhibitors of urease and α-glucosidase. Future Med Chem. 2024;16:2627–36. https://doi.org/10.1080/17568919.2024.2432303.
35. Cunha ES, Chen X, Sanz-Gaitero M, Mills DJ, Luecke H. Cryo-EM structure of *Helicobacter pylori* urease with an inhibitor in the active site at 2.0 Å resolution. Nat Commun. 2021;12:230. https://doi.org/10.1038/s41467-020-20485-6.

36. Bank RPD, RCSB PDB – 4GY7. accessed November 10, : Crystallographic structure analysis of urease from Jack bean (Canavalia ensiformis) at 1.49 A Resolution, (n.d.). https://www.rcsb.org/structure/4GY7 (2025).
37. Khan Y, Maalik A, Rehman W, Sarfraz H, Hussain R, Khan S, et al. Facile 3-chloro-1H-indazole based 1,3,4-thiadiazole derivatives as novel thymidine phosphorylase and anti-diabetic inhibitors: experimental, in-vitro and molecular modelling approaches. Naunyn Schmiedebergs Arch Pharmacol. 2025(1). https://doi.org/10.1007/s00210-025-04385-4.
38. Khan Y, Mukhtiar A, Sarfraz H, Khan S, Hussain R, Naeem MU, Sattar A, Aziz T, Panezai ZUR, Albekairi TH, Jabbir F. Unveiling of the novel benzothiazole derived thiazolidinone derivatives: in vitro and in silico insights to design a promising agent for anti-Alzheimer's disease. Z für Naturforschung C. 2025;81:75–93. https://doi.org/10.1515/znc-2024-0244.
39. Wang Y, Zhou Y, Khan FI. Molecular insights into structural dynamics and binding interactions of selected inhibitors targeting SARS-CoV-2 main protease. Int J Mol Sci. 2024;25:13482. https://doi.org/10.3390/ijms252413482.
40. Ahmed A, Zaib S, Bhat MA, Saeed A, Altaf MZ, Zahra FT, et al. Acyl pyrazole sulfonamides as new antidiabetic agents: synthesis, glucosidase inhibition studies, and molecular docking analysis. Front Chem. 2024;12:1380523. https://doi.org/10.3389/fchem.2024.1380523.
41. Fu L, Shi S, Yi J, Wang N, He Y, Wu Z, Peng J, Deng Y, Wang W, Wu C, Lyu A, Zeng X, Zhao W, Hou T, Cao D. ADMETlab 3.0: an updated comprehensive online ADMET prediction platform enhanced with broader coverage, improved performance, API functionality and decision support. Nucleic Acids Res. 2024;52:W422–31. https://doi.org/10.1093/nar/gkae236.
42. Sarfraz H, Rehman W, Rahim F, Khan S, Sardar A, Iqbal T, et al. Discovery and optimization of a novel series of pyrazole-linked oxadiazole conjugates as α-amylase inhibitors: in silico DFT, ADMET prediction, toxicological assessment and molecular docking insight. J Mol Struct. 2026;1351:144177. https://doi.org/10.1016/j.molstruc.2025.144177.
43. Zaib S, Rana N, Ali HS, Hussain N, Areeba HA, Ogaly FAM, Al-Zahrani I, Khan. Discovery of druggable potent inhibitors of serine proteases and farnesoid X receptor by ligand-based virtual screening to obstruct SARS-CoV-2. Int J Biol Macromol. 2023;253:127379. https://doi.org/10.1016/j.ijbiomac.2023.127379.
44. Ali HS, Warwicker J, de Visser SP. How does the nonheme iron enzyme NapI react through l-arginine desaturation rather than hydroxylation? A quantum mechanics/molecular mechanics study. ACS Catal. 2023;13:10705–21. https://doi.org/10.1021/acscatal.3c02262.
45. Ali HS, de Visser SP. Electrostatic perturbations in the substrate-binding pocket of Taurine/α-Ketoglutarate dioxygenase determine its selectivity. Chem Eur J. 2022;28:e202104167. https://doi.org/10.1002/chem.202104167.
46. Chen VB, Arendall WB, Headd JJ, Keedy DA, Immormino RM, Kapral GJ, et al. MolProbity: all-atom structure validation for macromolecular crystallography. Acta Crystallogr Sect D Biol Crystallogr. 2010;66:12–21. https://doi.org/10.1107/S0907444909042073.
47. Gordon JC, Myers JB, Folta T, Shoja V, Heath LS, Onufriev A. H++: a server for estimating p Ka s and adding missing hydrogens to macromolecules. Nucleic Acids Res. 2005;33:W368–71. https://doi.org/10.1093/nar/gki464.
48. Case DA, Aktulga HM, Belfon K, Ben-Shalom IY, Berryman JT, Brozell SR, et al. Amber 2023. University of California, San Francisco; 2023.
49. Tian C, Kasavajhala K, Belfon KAA, Raguette L, Huang H, Migues AN, et al. ff19SB: amino-acid-specific protein backbone parameters trained against quantum mechanics energy surfaces in solution. J Chem Theory Comput. 2020;16:528–52. https://doi.org/10.1021/acs.jctc.9b00591.
50. Träg J, Zahn D. Improved GAFF2 parameters for fluorinated alkanes and mixed hydro- and fluorocarbons. J Mol Model. 2019;25:39. https://doi.org/10.1007/s00894-018-3911-5.
51. Izadi S, Anandakrishnan R, Onufriev AV. Building water models: a different approach. J Phys Chem Lett. 2014;5:3863–71. https://doi.org/10.1021/jz501780a.
52. Joung IS, Cheatham TEI. Determination of alkali and halide monovalent ion parameters for use in explicitly solvated biomolecular simulations. J Phys Chem B. 2008;112:9020–41. https://doi.org/10.1021/jp8001614.
53. Loncharich RJ, Brooks BR, Pastor RW. Langevin dynamics of peptides: the frictional dependence of isomerization rates of N-acetylalanyl-N′-methylamide. Biopolymers. 1992;32:523–35. https://doi.org/10.1002/bip.360320508.
54. Lin Y, Pan D, Li J, Zhang L, Shao X. Application of Berendsen barostat in dissipative particle dynamics for nonequilibrium dynamic simulation. J Chem Phys. 2017;146:124108. https://doi.org/10.1063/1.4978807.
55. Ryckaert JP, Ciccotti G, Berendsen HJC. Numerical integration of the cartesian equations of motion of a system with constraints: molecular dynamics of n-alkanes. J Comput Phys. 1977;23:327–41. https://doi.org/10.1016/0021-9991(77)90098-5.
56. Miyamoto S, Kollman PA. Settle: an analytical version of the SHAKE and RATTLE algorithm for rigid water models. J Comput Chem. 1992;13:952–62. https://doi.org/10.1002/JCC.540130805.
57. Essmann U, Perera L, Berkowitz ML, Darden T, Lee H, Pedersen LG. A smooth particle mesh Ewald method. J Chem Phys. 1995;103:8577–93. https://doi.org/10.1063/1.470117.
58. Darden T, York D, Pedersen L. Particle mesh Ewald: an Nlog(N) method for Ewald sums in large systems. J Chem Phys. 1993;98:10089–92. https://doi.org/10.1063/1.464397.
59. Roe DR, Cheatham TEI. Software for processing and analysis of molecular dynamics trajectory data. J Chem Theory Comput. 2013;9:3084–95. https://doi.org/10.1021/ct400341p.
60. MDAnalysis. accessed November 10, : A toolkit for the analysis of molecular dynamics simulations - Michaud-Agrawal – 2011 - Journal of Computational Chemistry - Wiley Online Library, (n.d.). https://onlinelibrary.wiley.com/doi/full/10.1002/jcc.21787 (2025).
61. Humphrey W, Dalke A, Schulten K. VMD: visual molecular dynamics. J Mol Graph. 1996;14:33–8-27-8. https://doi.org/10.1016/0263-7855(96)00018-5.
62. S. L., The PyMOL Molecular Graphics System, Version 1.8., (2015). https://cir.nii.ac.jp/crid/1370576118684734988 (accessed November 10, 2025).
63. Artursson P, Karlsson J. Correlation between oral drug absorption in humans and apparent drug permeability coefficients in human intestinal epithelial (Caco-2) cells. Biochem Biophys Res Commun. 1991;175:880–5. https://doi.org/10.1016/0006-291X(91)91647-U.
64. Akash M, Zaib S, Ahmad M, Sultan S, Al-Hussain SA. Synthesis and biological evaluation of pyridylpiperazine hybrid derivatives as urease inhibitors. Front Chem. 2024. https://doi.org/10.3389/fchem.2024.1371377.


## Publisher's note